11-17-2020

Requisite chromatin remodeling for myeloid and erythroid lineage differentiation from erythromyeloid progenitors

Jun Wu

Karen Krchma

Hyung Joo Lee

Sairam Prabhakar

Xiaoli Wang

See next page for additional authors

Authors

Jun Wu, Karen Krchma, Hyung Joo Lee, Sairam Prabhakar, Xiaoli Wang, Haiyong Zhao, Xiaoyun Xing, Rho H Seong, Daved H Fremont, Maxim N Artyomov, Ting Wang, and Kyunghee Choi

Article

Requisite Chromatin Remodeling for Myeloid and Erythroid Lineage Differentiation from Erythromyeloid Progenitors

Graphical Abstract
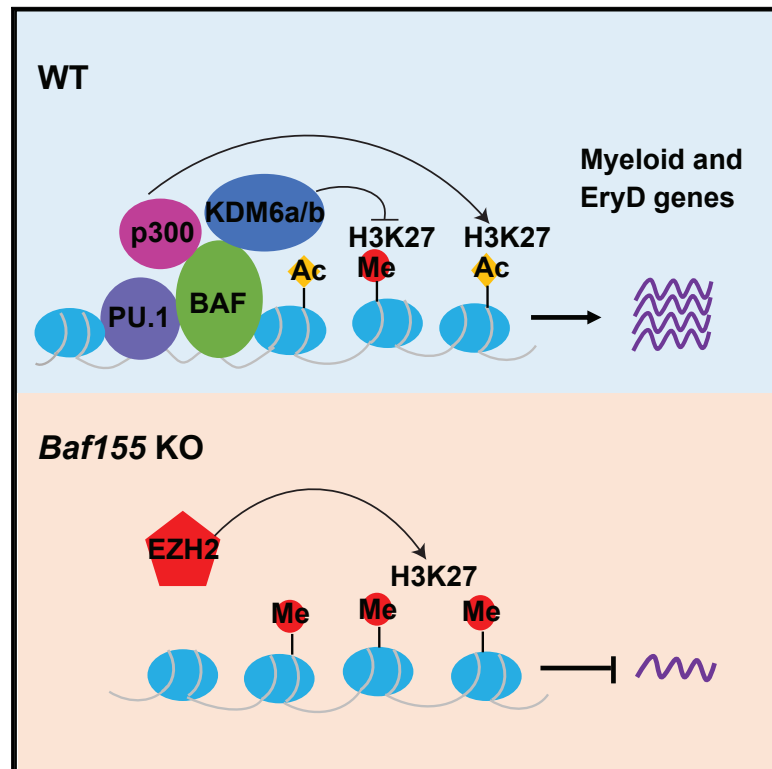
Authors

Jun Wu, Karen Krchma,
Hyung Joo Lee, ..., Maxim N. Artyomov,
Ting Wang, Kyunghee Choi

Correspondence

kchoi@wustl.edu

In Brief

The mammalian chromatin-remodeling BAF (BRG1/BRM-associated factor) complex has an essential role in developmental and pathological processes. Wu et al. show that BAF-mediated chromatin remodeling and activation of the myeloid and definitive erythroid transcriptional program at the EMP stage is critical for myeloid and definitive erythroid lineage development.

Highlights

- *Baf155* is required for yolk sac myeloid and definitive erythroid lineage development

- BAF-mediated chromatin remodeling of myeloid gene loci occurs at the EMP stage

- Inaccessible chromatin in *Baf155*-deficient EMPs is enriched by the ETS binding motif

- BAF155 interacts with PU.1 and is recruited to PU.1 target gene loci

CellPress

Article

Requisite Chromatin Remodeling for Myeloid and Erythroid Lineage Differentiation from Erythromyeloid Progenitors

Jun Wu,[1,7] Karen Krchma,[1,7] Hyung Joo Lee,[2,3] Sairam Prabhakar,[1] Xiaoli Wang,[1] Haiyong Zhao,[1] Xiaoyun Xing,[2,3] Rho H. Seong,[4] Daved H. Fremont,[1] Maxim N. Artyomov,[1] Ting Wang,[2,3,6] and Kyunghee Choi[1,5,8,*]

[1]Department of Pathology and Immunology, Washington University School of Medicine, St. Louis, MO, USA
[2]Department of Genetics, Washington University School of Medicine, St. Louis, MO, USA
[3]Edison Family Center for Genome Sciences and Systems Biology, Washington University School of Medicine, St. Louis, MO, USA
[4]Department of Biological Sciences, Institute of Molecular Biology and Genetics, Seoul National University, Seoul, Korea
[5]Graduate School of Biotechnology, Kyung Hee University, Yong In, Korea
[6]McDonnell Genome Institute, Washington University School of Medicine, St Louis, MO, USA
[7]These authors contributed equally
[8]Lead Contact
*Correspondence: kchoi@wustl.edu
https://doi.org/10.1016/j.celrep.2020.108395

SUMMARY

The mammalian SWitch/Sucrose Non-Fermentable (SWI/SNF) chromatin-remodeling BAF (BRG1/BRM-associated factor) complex plays an essential role in developmental and pathological processes. We show that the deletion of *Baf155*, which encodes a subunit of the BAF complex, in the Tie2(+) lineage (*Baf155* (CKO) leads to defects in yolk sac myeloid and definitive erythroid (EryD) lineage differentiation from erythromyeloid progenitors (EMPs). The chromatin of myeloid gene loci in *Baf155* CKO EMPs is mostly inaccessible and enriched mainly by the ETS binding motif. BAF155 interacts with PU.1 and is recruited to PU.1 target gene loci together with p300 and KDM6a. Treatment of *Baf155* CKO embryos with GSK126, an H3K27me2/3 methyltransferase EZH2 inhibitor, rescues myeloid lineage gene expression. This study uncovers indispensable BAF-mediated chromatin remodeling of myeloid gene loci at the EMP stage. Future studies exploiting epigenetics in the generation and application of EMP derivatives for tissue repair, regeneration, and disease are warranted.

INTRODUCTION

The mammalian hematopoietic system is established from multiple embryonic origins. The first tissue to produce blood cells is the yolk sac, which generates primitive erythroid (EryP) cells and megakaryocytes (MegPs) presumably from bipotential MegP erythroid progenitors (pMEPs) (Tober et al., 2007). Although EryPs, which express embryonic globin genes, can be detected as early as embryonic day 7.25 (E7.25) in the blood islands of the yolk sac, mature MegP cells are not detected until later, around E9.5, in the yolk sac (Tober et al., 2007). The primary function of EryP cells is to provide developing embryos with oxygen and nutrients to accommodate the rapid growth of the embryo. Until recently, hematopoietic stem cells (HSCs) originating from the hemogenic endothelium of the aorta-gonad-mesonephros (AGM) have been thought to initiate definitive hematopoiesis. However, this paradigm has been challenged by the identification of erythromyeloid progenitors (EMPs), which generate definitive erythroid (EryD) and myeloid cell lineages before the establishment of HSCs (Hoeffel and Ginhoux, 2018; McGrath et al., 2015; Ginhoux et al., 2010; Schulz et al., 2012;

Hashimoto et al., 2013; Gomez Perdiguero et al., 2015). EMPs develop transiently from the *Tie2*-expressing hemogenic endothelium of the yolk sac around E8.5–E10.5, migrate to the fetal liver, expand, and provide embryos with EryD and myeloid cells in fetal life (Chen et al., 2011; McGrath et al., 2015; Gomez Perdiguero et al., 2015; Palis, 2016). EMPs are ultimately replaced by HSCs, which generate a full spectrum of blood cells, including lymphoid cell lineages. The importance of EMPs was realized by the finding that tissue-resident macrophages originate from EMPs through monocyte intermediates, although microglia are believed to originate from yolk sac macrophages (Ginhoux et al., 2010). Despite the critical establishment of the cellular origin of tissue-resident macrophages from EMPs, few studies have examined the molecular mechanisms that regulate myeloid and EryD differentiation from EMPs.

In eukaryotes, DNA is packaged into nucleosomes and subsequent higher-order chromatin structures. As a result, DNA is not easily accessible for transcriptional machinery. Two fundamental mechanisms that allow cells to respond to signals and trigger gene expression are chromatin remodeling and histone modification. Transcription factors and other proteins are

believed to gain access to nucleosome-bound DNA using ATP-dependent chromatin-modifying and remodeling enzymes, such as the SWI/SNF complex family (Hargreaves and Crabtree, 2011; Kadoch and Crabtree, 2015). SWI/SNF complexes, by utilizing energy derived from ATP hydrolysis, destabilize histone-DNA interactions and create an open chromatin state. SWI/SNF complexes are composed of one core ATPase (Brg1 or Brm) and distinct paralogous BRG1/BRM-associated factor (BAF) subunit family members that can interact with cofactors, including transcription factors. Combinatorial assembly of alternative families of subunits confers functional specificity to BAF complexes in different tissues and cell types (Wu et al., 2009). A recent study showing that BAF60c, a subunit of BAF critical for heart development (Lickert et al., 2004), together with GATA4 and TBX5, can reprogram mesoderm to cardiomyocytes in the mouse embryo (Takeuchi and Bruneau, 2009) highlights the fact that SWI/SNF-mediated chromatin remodeling is integral to the lineage-specific transcriptional network. Notably, enforced expression of just one component of the multi-protein BAF complex, BAF60c, in that study was sufficient to confer lineage-specific gene regulation.

Although chromatin-remodeling proteins are critical for establishing cell lineage specification in mammalian development, functional details of how these proteins affect specific cell lineage development are still lacking. Gene knockout studies have demonstrated that BRG1 ATPase and BAF155 are required for blood and vascular development. Particularly, *Brg1*- or *Baf155*-deficient embryos die around implantation (Bultman et al., 2000; Kim et al., 2001). The peri-implantation lethality of *Baf155*-deficient embryos can be extended to mid-gestation by *Baf155* transgene expression (*Baf155⁻/⁻; Tg⁺*). However, these animals display severe blood vessel formation defects in the yolk sac around E10.5 (Han et al., 2008). Moreover, *Tie2-Cre; Brg1^{f/f}* mice are embryonic lethal because of apoptosis of EryP and lack of embryonic globin gene expression (Griffin et al., 2008). Angiogenesis is also defective in these animals. While these studies demonstrate the critical role of BAF-mediated chromatin remodeling in EryP and angiogenesis, it remains unclear whether BAF-mediated chromatin remodeling is subsequently required for the yolk sac hematopoiesis. In this study, we determined BAF-mediated chromatin remodeling requirements from hemogenic endothelium to EMPs and myeloid and EryD lineage differentiation by deleting *Baf155* in the *Tie2* lineage. Our data demonstrate that BAF155-mediated chromatin remodeling of myeloid and EryD gene loci at the EMP stage is critical for activation of the myeloid and EryD transcriptional program as well as myeloid and EryD lineage differentiation.

RESULTS

### *Baf155* CKO Mice Are Embryonic Lethal, Showing Defects in Myeloid and EryD Lineage Development

To assess the role of chromatin remodeling in hematopoietic lineage development downstream of the yolk sac hemogenic endothelium, we first generated *Tie2-Cre;Baf155^{f/+}* mice from matings between *Baf155^{f/f}* (Choi et al., 2012) and *Tie2-Cre* mice, which have been shown to target the yolk sac hemogenic endothelium (Chen et al., 2011; Gomez Perdiguero et al., 2015).

We also observed effective tdTomato expression in EryP cells, endothelial cells, myeloid cells, and microglia in *Tie2-Cre;R-osa-loxp-stop-loxp-tdTomato* yolk sac and brain (Figure S1A). *Tie2-Cre;Baf155^{f/+}* mice were then crossed with *Baf155^{f/f}* mice to generate *Tie2-Cre;Baf155^{f/f}* mice (hereafter called *Baf155* CKO). We found no live *Baf155* CKO mice at weaning (Table S1). We found no *Baf155* CKO embryos with abnormal morphology up to E9.5. However, at E10.5, some *Baf155* CKO embryos were smaller compared with littermate controls and displayed occasional hemorrhage around the distal end of the tail and yolk sac (8 of 49), suggesting abnormal vessel formation. This is consistent with previous findings that *Brg1* or *Baf155* deficiency leads to angiogenesis defects (Griffin et al., 2008; Han et al., 2008). All *Baf155* CKO embryos showed severe growth retardation and seemingly abnormal gross morphology at E13.5 (data not shown).

We assessed whether the embryonic lethality in *Baf155* CKO mice was due to hematopoietic defects. Ter119⁺ erythroid cells from E9.5 and E10.5 yolk sacs, predominantly EryP cells at this stage, were present at similar levels in wild-type and *Baf155* CKO yolk sacs (Figures 1A and S1B). CD45⁻CD31⁺ endothelial cells were also present similarly in wild-type and CKO yolk sacs (Figures 1A and S1B). Notably, there was a significant reduction in myeloid cells, CD45⁺CD11b⁺, in *Baf155* CKO yolk sacs (Figures 1A and S1B). Yolk sac macrophages, CD45⁺F4/80⁺, as well as microglia of the brain, CD45⁺CX3CR1⁺CD11b⁺, were also reduced significantly in *Baf155* CKO embryos (Figures 1A, S1B, and S1C). Although EryP progenitors from wild-type littermate control and *Baf155* CKO yolk sacs were present similarly, myeloid progenitors and BFU-Es were decreased significantly in *Baf155* CKO yolk sacs (Figure 1B). Corroborating these data, expression of myeloid lineage genes, including *Irf8*, *Cx3cr1*, and *Fcgr3* (CD16), was reduced significantly in *Baf155* CKO yolk sacs (Figures 1C and S1D). However, genes expressed in the EryP lineage, *Klf1*, *Hbb-bh1*, and *Hbz*, were detected similarly in wild-type and CKO yolk sacs (Figure 1C). Genes expressed in EMPs, *cKit*, *Gata2*, *Tal1/Scl*, and *Myb*, were also detected similarly in E9.5 wild-type (WT) and *Baf155* CKO yolk sacs (Figure 1C). *GP1bb* (CD42c), *Mpl*, and *Itga2b* (CD41), genes expressed in megakaryocytes, were also expressed similarly in WT and CKO yolk sacs (Figure 1C). These results suggest that *Baf155* deficiency leads to selective defects in myeloid and EryD lineage development.

EMPs Develop in the Absence of *Baf155*

The selective myeloid and EryD lineage defects seen in *Baf155* CKO yolk sacs might be due to defects in EMP generation. Alternatively, EMPs are generated, but their differentiation might be blocked. To differentiate these two possibilities, we first analyzed EMPs based on phenotypic markers in *Baf155* CKO yolk sacs. EMPs are enriched in cKIT⁺CD41⁺CD16/32⁺ cells (McGrath et al., 2015). Because expression of *Fcgr3* encoding CD16 was clearly decreased in *Baf155* CKO yolk sacs (Figure 1C), we reasoned that inclusion of CD16/32 in the EMP analysis might be inadequate for measuring EMPs from *Baf155* CKO yolk sacs. Indeed, the cKIT⁺CD16/32⁺CD41⁺ or CD16/32⁺CD41⁺ cell population was reduced greatly in *Baf155* CKO yolk sacs (Figure S2). Because cKIT is critical for EMP
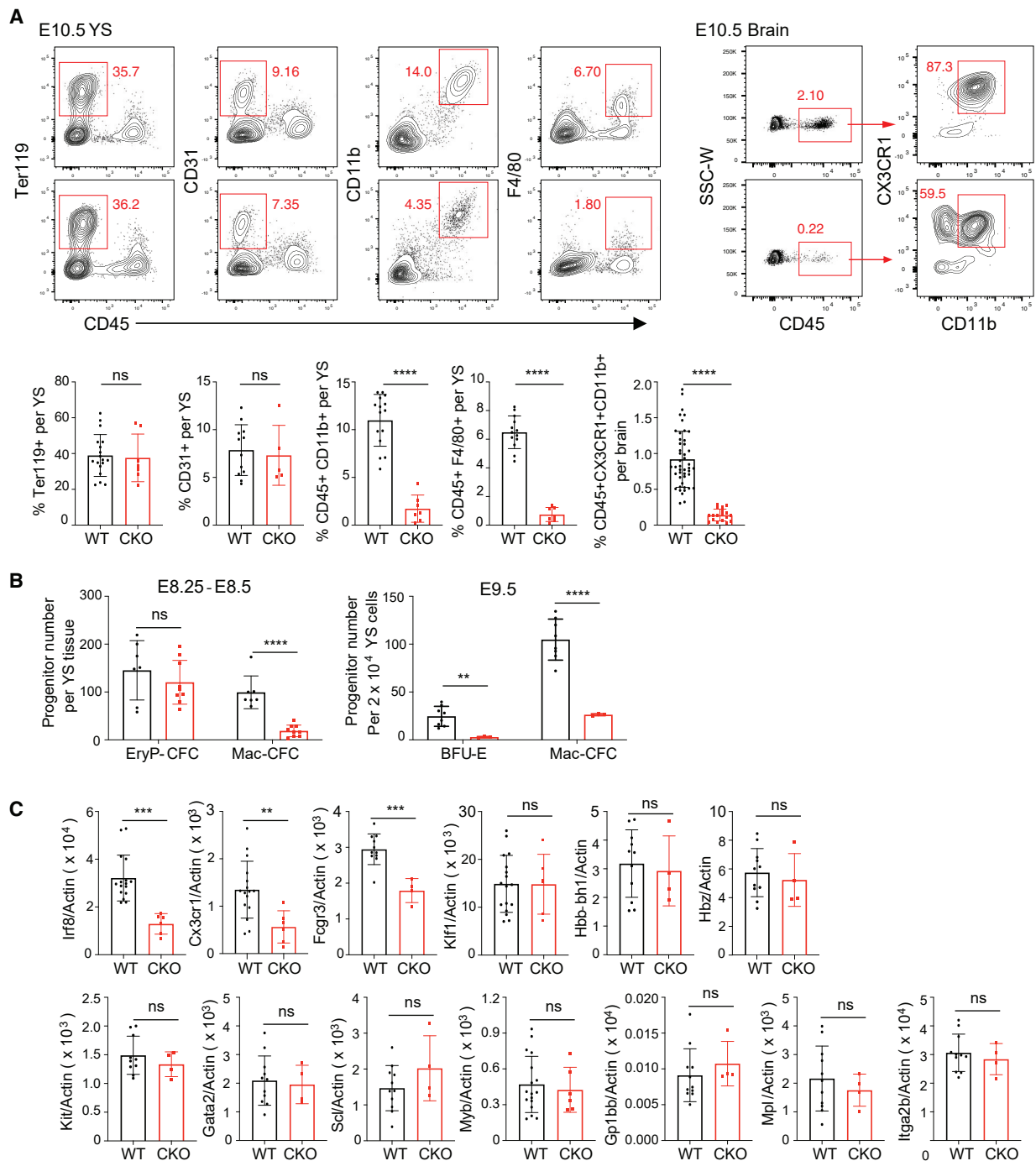
Figure 1. *Baf155* CKO Mice Show Defects in Myeloid and EryD Lineage Development

(A) A representative flow cytometry analysis of E10.5 yolk sacs (YS) EryP cells (CD45⁻Ter119⁺), ECs (CD45⁻CD31⁺), myeloid cells (CD45⁺CD11b⁺), macrophages (CD45⁺F4/80⁺), and brain microglia (CD45⁺CX3CR1⁺CD11b⁺) in wild-type (WT) and *Baf155* CKO mice is shown in the top panel. The percentage of each population is shown in the bottom panel. At least 5 biological replicates in 4 independent experiments for either genotype were analyzed, each representing an individual YS. Data are presented as mean ± SD. Student's t test; ns, not significant; ****p < 0.0001.

(B) Distribution of EryP (EryP-CFC), EryD (BFU-E), and macrophage (Mac-CFC) progenitors from E8.25–E8.5/E9.5 WT and *Baf155* CKO YS cells. E8.25–E8.5 data from 7 WT and 9 *Baf155* CKO biological replicates and E9.5 data from 8 WT and 3 *Baf155* CKO biological replicates representing two independent experiments, with each replicate consisting of a single YS, are shown. Data are presented as mean ± SD. Student's t test; **p < 0.005, ****p < 0.0001.

(C) qRT-PCR analysis of the indicated gene expression in E9.5 WT and *Baf155* CKO YS cells is shown. Data are presented as mean ± SD. Student's t test; **p < 0.005, ***p < 0.001.

See also Figure S1.
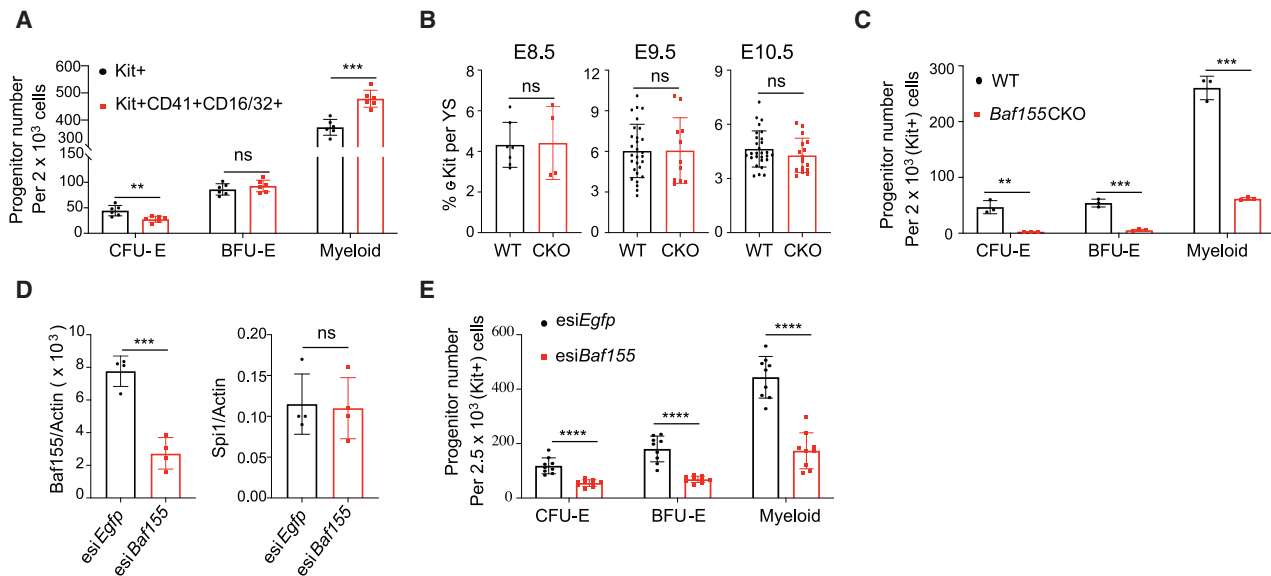
Figure 2. *Baf155* Is Required for Myeloid and EryD Lineage Differentiation from EMPs

(A) Distribution of CFU-E, BFU-E, and myeloid colonies developing from KIT$^+$ and KIT$^+$CD41$^+$CD16/32$^+$ population from WT E10.5 YSs. Data are presented as mean ± SD. Student's t test; **p < 0.005, ***p < 0.001; 6 biological replicates.

(B) Flow cytometry analysis of the cKIT$^+$ population per YS from WT and *Baf155* CKO embryos on the indicated embryonic day. E8.5 data (mean ± SD) are from 2 independent experiments. E9.5 and E10.5 data (mean ± SD) are from 6 independent experiments, each representing a single YS. Data are presented as mean ± SD. Student's t test.

(C) CFU-E, BFU-E, and myeloid colonies from cKIT$^+$ cells from WT (n = 3) and *Baf155* CKO (n = 3) YSs. Data are from 2 independent experiments, with each replicate consisting of a single or 2 pooled YSs of the same genotype. Data are presented as mean ± SD. Student's t test; **p < 0.01, ***p < 0.001.

(D) qRT-PCR analysis of the indicated gene expression in cKIT$^+$ cells from E10.5 WT YSs transfected with esiRNA against *Baf155* or *Egfp*. Data are presented as mean ± SD. Student's t test; ***p < 0.001; four biological replicates from 3 independent experiments.

(E) CFU-E, BFU-E, and myeloid colonies from cKIT$^+$ cells from E10.5 WT YSs transfected with esiRNA against *Baf155* or *Egfp*. Data are presented as mean ± SD. Student's t test; ***p < 0.001. Nine biological replicates from 3 independent experiments.

See also Figure S2.

development (Azzoni et al., 2018), and *cKit* expression was similar in WT and CKO yolk sacs (Figure 1C), we sorted cKIT$^+$ cells and evaluated their myeloid and EryD potential compared with cKIT$^+$CD41$^+$CD16/32$^+$ cells. There was an ~80% overlap between cKIT$^+$ and cKIT$^+$CD16/32$^+$CD41$^+$ cell populations (data not shown). Although cKIT$^+$ and cKIT$^+$CD41$^+$CD16/32$^+$ cells generated similar levels of BFU-Es, cKIT$^+$ cells generated slightly more CFU-Es compared with cKIT$^+$CD41$^+$CD16/32$^+$ cells, suggesting that cKIT$^+$ cells also contain more committed erythroid progenitors (Figure 2A). Slightly more myeloid colonies were generated from cKIT$^+$CD41$^+$CD16/32$^+$ cells compared with cKIT$^+$ cells, suggesting that cKIT$^+$CD41$^+$CD16/32$^+$ cells also enrich committed myeloid progenitors (Figure 2A). Importantly, cKIT$^+$ cells were present at similar levels in WT and *Baf155* CKO yolk sacs at E8.5–E10.5 (Figure 2B). However, cKIT$^+$ cells from E10.5 *Baf155* CKO yolk sacs generated significantly fewer myeloid or BFU-E colonies compared with controls (Figure 2C), suggesting that EMPs were generated in *Baf155* CKO embryos but that *Baf155* CKO EMPs have a block in myeloid and EryD differentiation. We assessed whether *Baf155* inhibition in EMPs was sufficient to block myeloid and EryD differentiation. To this end, we knocked down *Baf155* in EMPs by transfecting Baf155 esiRNA into sorted cKIT+ cells. We achieved more than 60% KD efficiency of *Baf155* expression, whereas expression of irrel-

evant genes, such as *Pu.1*, was unaffected (Figure 2D). Notably, myeloid and EryD output from EMPs was reduced greatly by *Baf155* knockdown (KD) (Figure 2E), indicating that acute deletion of *Baf155* in EMPs is sufficient to inhibit myeloid and EryD lineage differentiation. These data collectively suggest that *Baf155*-mediated chromatin remodeling at the EMP stage is critical for efficient downstream myeloid and EryD lineage differentiation.

Single-Cell RNA Sequencing Reveals Myeloid Lineage Differentiation Defects of *Baf155*-Deficient EMPs

To better understand the myeloid lineage differentiation block in *Baf155* CKO embryos, we subjected yolk sacs from WT and *Baf155* CKO mice to single-cell RNA sequencing (scRNA-seq). After filtering out low-quality cells, 722 WT and 791 *Baf155* CKO yolk sac cells were chosen for further analysis. t-stochastic neighbor embedding (t-SNE) was used to visualize the populations. WT yolk sac cells were clustered into 7 populations based on similarities of the transcriptome (Figure S3A). High expression of *Kdr*, *Cdh5*, and *Pecam1* highlights cluster 5 to be an endothelial cell population (Figure S3B). Two distinct erythroid cell populations were visible based on the erythroid lineage markers *Gata1*, Klf1, and *EpoR* (Figure S3C). Expression of *Hbb-y*, *Hbb-x*, and *Hbb-bh1* (embryonic β-globin genes) separated

cluster 2 as primitive and cluster 4 as an EryD cell population (Figure S3D). We also identified *Gm15915*, *Ccl17*, *Muc13*, and *Gdf3* to be expressed in an EryD-specific manner (Figures S3E and S3I). Expression of the mature myeloid lineage genes *Trem2*, *Emr1*, *Cx3cr1*, *Csf1r*, *Irf8*, and *Cd68* identified cluster 6 as a myeloid cell population (Figures S3F and S3J). Enriched expression of *cKit* and *Itga2b*, encoding CD41, and *Cd34* identified cluster 0 as EMPs (Figure S3G). Expression of *Pu.1* (Spi1), a critical factor for myeloid lineage development, expression was high in EMPs, and its expression was detected continuously in the myeloid lineage arm (Figures S3G and S3K). *Bcl11a*, *Myb*, *Scl* (Tal1), and *Gata2* expression was detected in EMPs, and their expression was detected continuously in the EryD cell cluster (Figure S3K). It is also notable that *Baf155* and *Cd34* expression was high in the EMP population (Figure S3M). As we reported recently (Zhao and Choi, 2019), clusters 1 and 3 represent smooth muscle cells and pericytes, based on *Hand1*, *Hand2*, *Acta2*, *Tbx20*, and *Cd248* expression (Figures S3H and S3L). *Desmin* expression separated pericytes (cluster 3) from smooth muscle cells (cluster 1; Figure S3L).

When we overlaid WT and *Baf155* CKO scRNA-seq data, we observed that the transcriptomes of endothelial cells (ECs; Figure 3A, cluster 7), EryP cells (Figure 3A, clusters 1 and 6), and smooth muscle cells and pericytes (Figure 3A, clusters 2, 4, 5, and 8) overlapped each other, indicating that *Baf155* deficiency did not affect their overall transcriptome (Figures 3A–3D). However, clusters 0 and 3, both expressing EMP genes (Figures 3E and 3F), showed clear separation between WT and *Baf155* CKO yolk sac cells (Figures 3B–3D). *Baf155* expression was clearly absent in cluster 3, indicating that *Baf155* was deleted effectively in this population (Figure 3B). Strikingly, a population with the mature myeloid gene signature (cluster 9) was readily visible in WT yolk sacs but absent in *Baf155* CKO yolk sacs (Figures 3E and 3G). A population with the EryD gene signature was also reduced greatly in *Baf155* CKO yolk sacs (Figures 3E and 3H). Intriguingly, although EryD cells were reduced greatly, the megakaryocytic lineage gene signature was high in the presumptive *Baf155* CKO EryD cell population (Figure 3I). This suggests that the megakaryocytic lineage may be the default pathway in EryD and megakaryocytic lineage choice and that chromatin remodeling is also critical for EryD and megakaryocyte lineage bifurcation. Additionally, endothelial genes were still expressed in the *Baf155* CKO EMP cell population (Figure 3J). These data collectively suggest that chromatin remodeling is needed at the EMP stage for further differentiation into myeloid and EryD lineages to occur. The endothelial gene program is sustained in EMPs when subsequent differentiation is blocked. Alternatively, termination of the endothelial gene program might require chromatin remodeling.

Chromatin Accessibility of Myeloid and EryD Gene Loci Is Reduced Greatly in *Baf155* CKO EMPs

So far, the data suggested that *Baf155* deficiency leads to myeloid and EryD differentiation block from EMPs. To better understand the myeloid lineage differentiation defect in *Baf155*-deficient EMPs, we sorted cKIT$^+$ cells, EMP enriched, from WT and *Baf155* CKO yolk sacs (Figure S4A) and assessed genome-wide chromatin accessibility by assay for transpo-

sase-accessible chromatin using sequencing (ATAC-seq; Buenrostro et al., 2013). We identified 103,043 and 143,021 accessible chromatin regions in *Baf155* CKO and WT cKIT$^+$ cells, respectively. Among these ATAC-seq peaks, 7,422 regions were more accessible in WT than in *Baf155* CKO cells, whereas only 56 regions were more accessible in *Baf155* CKO cells than in WT cells (Figures 4A and 4B). The differentially accessible genomic regions (DARs) were enriched for the binding motifs of transcription factors (TFs) such as PU.1, IRF8, AP-1, and CEBP, whereas 13,213 unaffected accessible genomic regions, commonly open in CKO and WT EMPs (fold change < 1.1 and p > 0.05), were enriched for the different TF binding motifs, such as CTCF (Figures 4B, 4C, and S4B). Of the 7,422 DARs specific to WT EMPs, 3,679 peaks contained PU.1 motifs, whereas 1,472 of 13,213 unaffected peaks contained PU.1 motifs. This suggests that loss of *Baf155* leads to a closed chromatin structure at selective genomic regions. The data also suggest potential interplay between ETS factors and BAF-mediated chromatin remodeling in activating the myeloid lineage program.

The genes associated with selective genomic regions with loss of chromatin accessibility in *Baf155* CKO EMPs were enriched for biological functions related to immune responses, including inflammatory response and myeloid leukocyte activation, whereas genes with unaffected accessible regions were enriched for biological functions different from those (Figure 4D). Genes under the inflammatory response and myeloid leukocyte activation categories mainly include myeloid genes such as *Cx3cr1*, *Trem2*, *Csf1r*, *Irf8*, *Emr1*, and *Fcgr3* (CD16). Importantly, chromatin of these gene loci was largely inaccessible in *Baf155* CKO EMPs (Figures 4E and S4C), explaining the block of myeloid lineage differentiation. In contrast, EC gene loci, *Kdr*, *Cdh5*, and *Esam*, were similarly accessible in WT and *Baf155* CKO EMPs (Figure S4D). EMP gene loci, *cKit*, *Itga2b* (*Cd41*), and *Cd34*, were also readily accessible in WT and *Baf155* CKO EMPs (Figure S4E). Importantly, although chromatin of erythroid lineage genes that were commonly expressed in EryP cells was readily accessible, chromatin of the erythroid lineage genes that were specifically upregulated in EryD cells, *Hbb-bt*, *Gm15915*, and *Gdf3*, were not (Figure 4F). These data suggest that BAF155-mediated chromatin remodeling of myeloid and EryD gene loci at the EMP stage is necessary for subsequent myeloid and EryD lineage differentiation.

BAF155 Is Recruited to PU.1 Target Gene Loci

PU.1 is a master ETS factor critical for myeloid lineage development. PU.1 regulates its own expression (Chen et al., 1995), although the mechanisms of this autoregulation have not been elucidated clearly. Because reduced accessible regions in *Baf155* CKO EMPs are represented predominantly by the ETS binding motif, we assessed whether PU.1 requires the BAF complex for activating the myeloid lineage program. Intriguingly, *Pu.1* expression itself was diminished in CKO yolk sacs (Figure 5A). Chromatin of the *Pu.1* locus was less accessible in CKO EMPs (Figure 5A). Because *Baf155* KD in EMPs could block myeloid and EryD differentiation without affecting *Pu.1* expression (Figures 2D and 2E), we reasoned that diminished expression of *Pu.1* and its target genes in *Baf155* CKO yolk sacs could be due to deficiency of BAF-mediated chromatin remodeling at
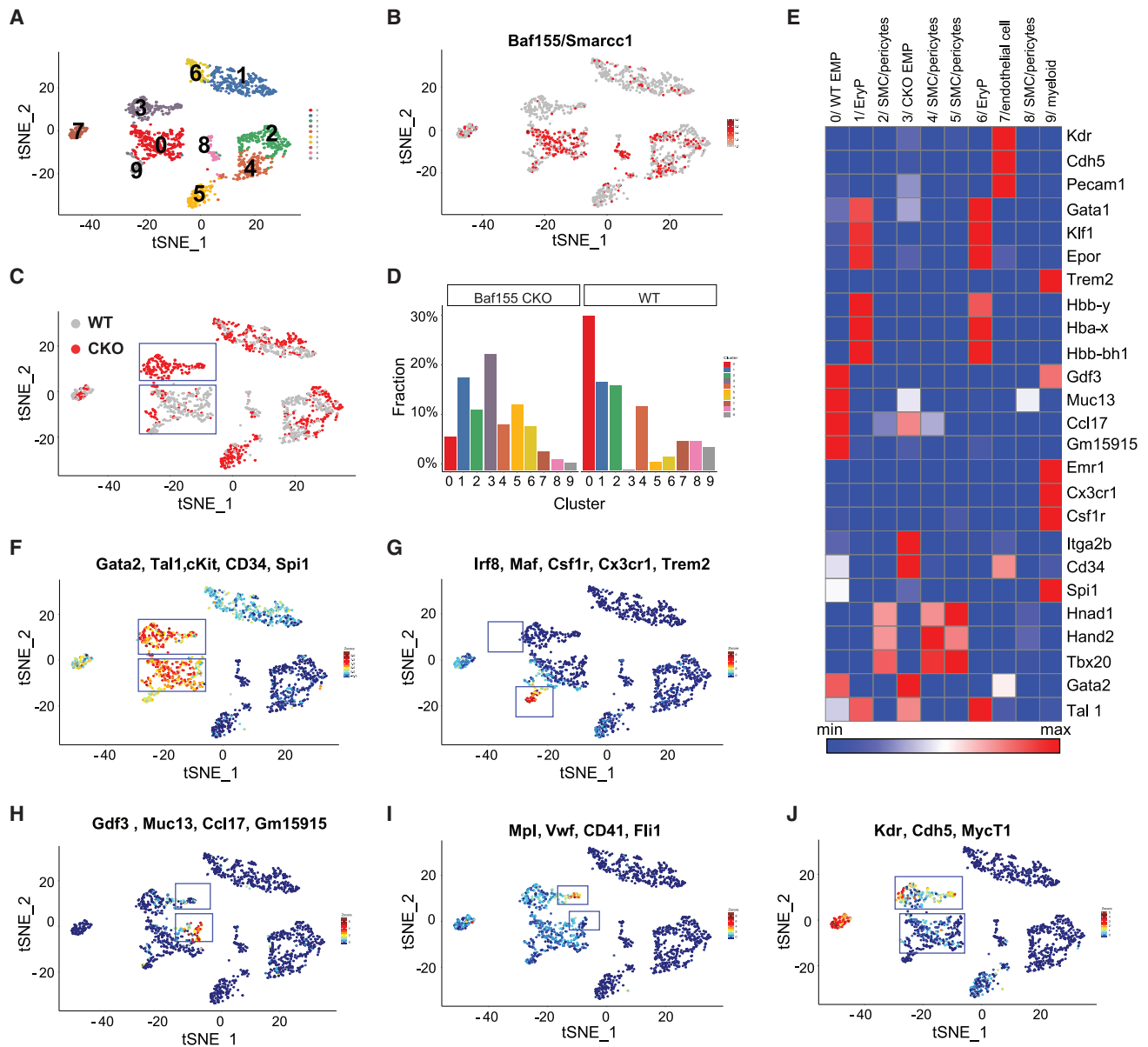
Figure 3. scRNA-Seq Data Reveal Myeloid and EryD Differentiation Defects from *Baf155*-Deficient EMPs

(A) t-SNE projection of all cells, showing 10 different clusters.

(B) *Baf155/Smarcc1* expression in all YSs, showing the absence of *Baf155* expression in the CKO EMP cell population.

(C) An overlay of scRNA-seq data between WT and *Baf155* CKO YSs.

(D) Percentage of cells in each cluster from WT versus *Baf155* CKO YSs.

(E) Heatmap showing differentially expressed genes in each cluster.

(F) The EMP signature genes *Gata2*, *Tal1*, *cKit*, *Cd34*, and *Pu.1/Spi1* are similarly expressed in WT and *Baf15*5 CKO EMPs.

(G) A cell population with myeloid lineage signature gene expression (*Irf8*, *Maf*, *Csf1r*, *Cx3cr1*, and *Trem2*) is absent in *Baf155* CKO YSs.

(H) A cell population with EryD lineage signature genes expression (*Gdf3*, *Muc13*, *Ccl17*, and *Gm15915*) is significantly lower in *Baf155* CKO YSs.

(I) A population with elevated megakaryocyte lineage signature gene expression is increased in *Baf155* CKO YS cells.

(J) Endothelial lineage signature genes are still expressed in the *Baf155*-deficient EMP cell population.

See also Figure S3.

Pu.1 and its target gene loci. We first assessed whether BAF155 is recruited to PU.1 target genes. We selected 7 genomic regions that contain the ETS motif and are differentially accessible in WT and Baf155 CKO yolk sacs. These include genomic regions that

are associated with the *Cx3cr1*, *Trem2*, *Csf1r*, *Irf8*, and *Cd68* genes (Figure 5B; Table S3). We also selected 2 unaffected ETS regions, UER1 and UER2, from the 1,472 peaks that contain the PU.1 motif but whose chromatin accessibility is unaffected
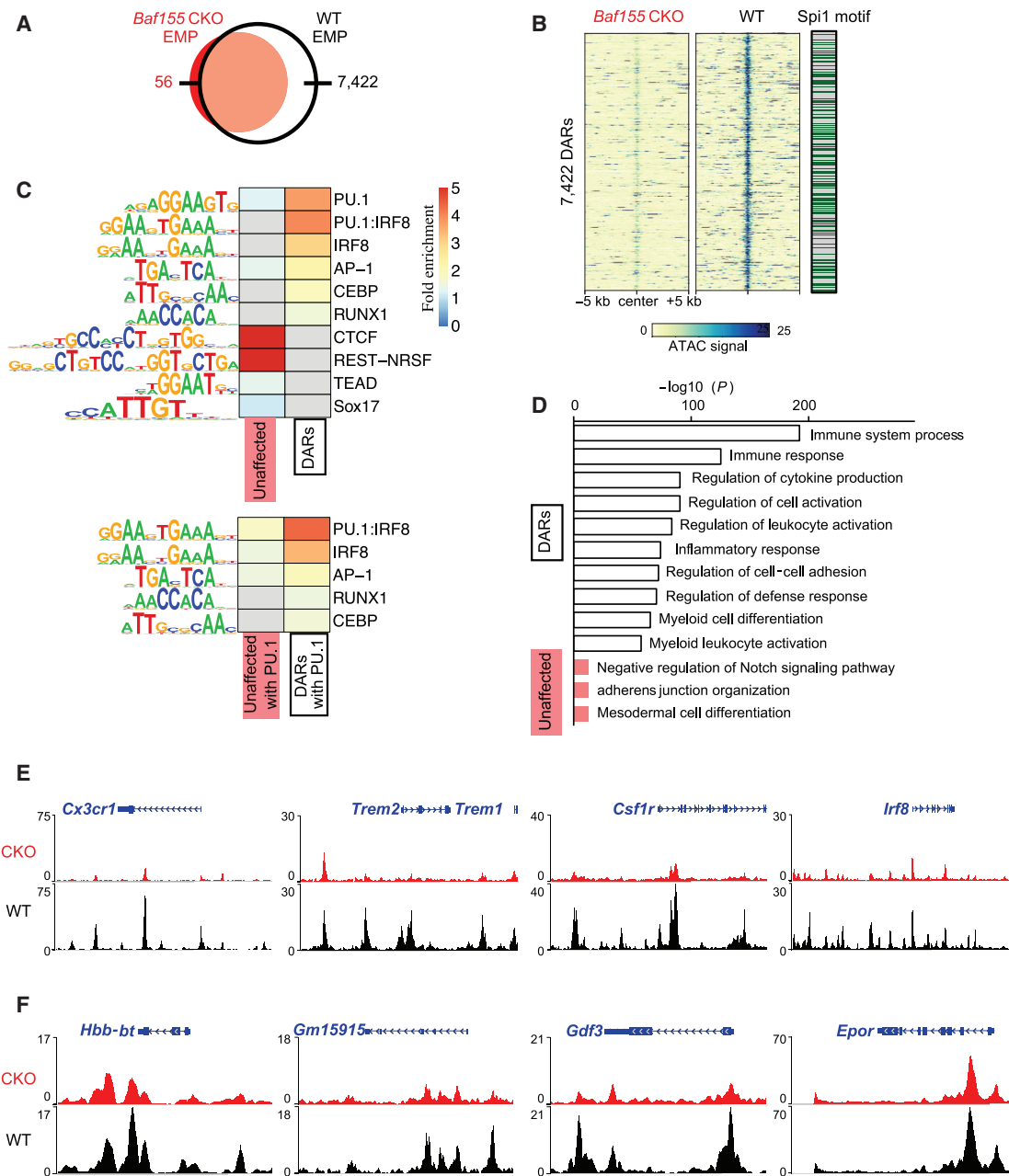
Figure 4. *Baf155* CKO EMPs Have Reduced Chromatin Accessibility at the Myeloid and EryD Gene Loci

(A) A Venn diagram of the numbers of ATAC-seq peaks found in *Baf155* CKO and WT EMPs.

(B) ATAC-seq signals over 10-kb regions centered on the differentially accessible regions (DARs) with reduced signals in *Baf155* CKO EMPs compared with the WT (left) and the presence of the *Spi1/Pu.1* motif in the DARs (right).

(C) Heatmaps of HOMER known TF motif fold enrichment in the DARs and unaffected accessible regions. Gray cells indicate no enrichment found (p > 0.05).

(D) Enriched Gene Ontology (GO) terms and their binomial p values from analyzing the DARs with reduced signals in *Baf155* CKO EMPs (white) and the unaffected peaks (red) using GREAT.

(E) Epigenome browser views of representative myeloid gene loci.

(F) Epigenome browser views of representative erythroid gene loci.

See also Figure S4.

by *Baf155* deficiency (Figure 5B; Table S3). Although a significant mean enrichment was observed for PU.1 and BAF155 binding at these PU.1 target gene loci, only BAF155 binding, not PU.1, was enriched at UER1 and UER2 (Figure 5B). We next determined whether BAF155 can form a complex with PU.1. Specifically, we generated a mouse embryonic fibroblast (MEF)
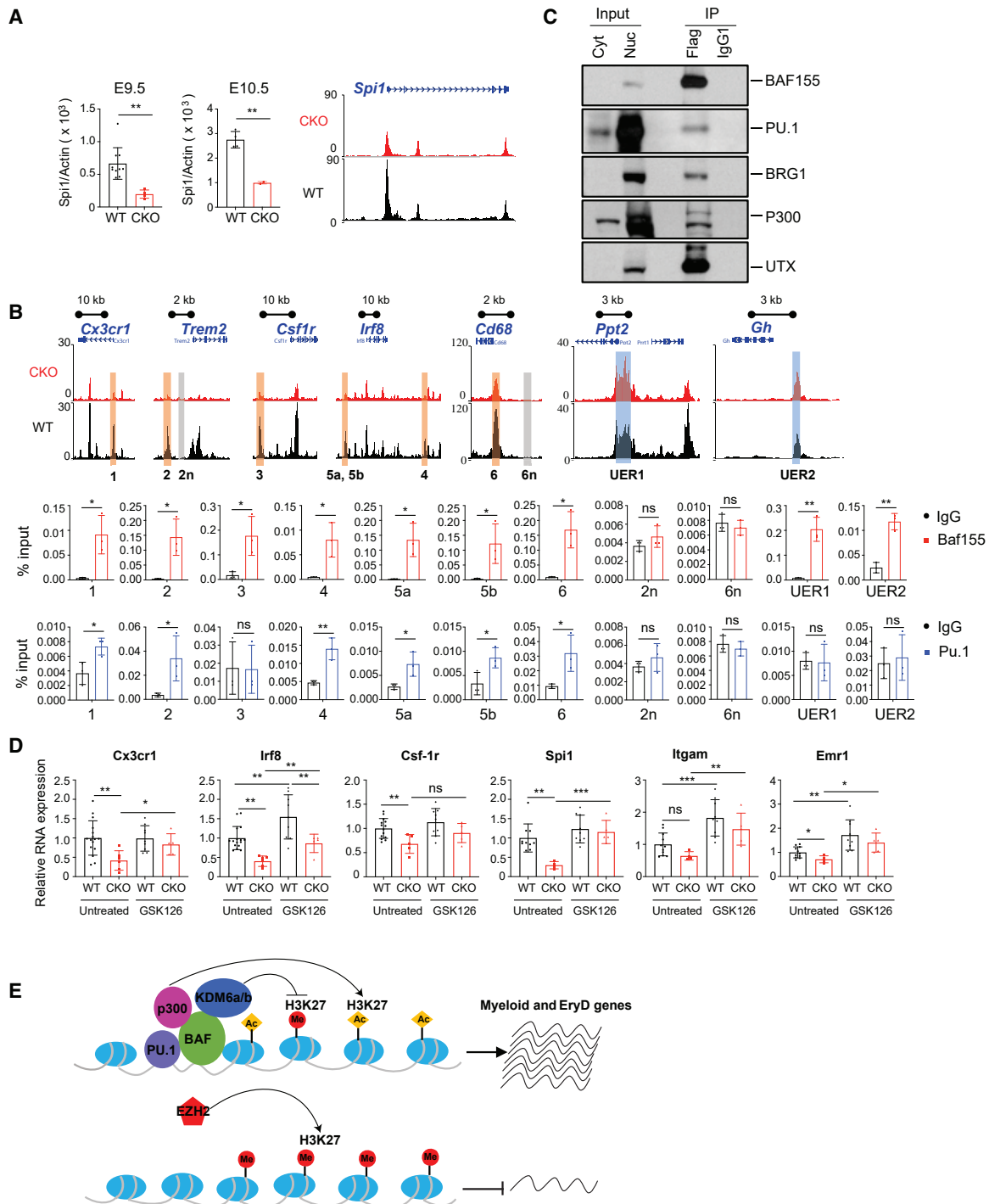
Figure 5. BAF155 Interacts with PU.1 and Is Recruited to Its Target Genes

(A) qRT-PCR analysis of *Pu.1* expression (top) and epigenome browser view of the *Spi1/Pu.1* locus (bottom) from WT and *Baf155* CKO YSs. Data are from at least two biological replicates for either genotype, with each replicate consisting of an individual YS. Data are presented as mean ± SD. Student's t test; **p < 0.01.

(B) Epigenome browser views of selected myeloid and negative control genomic regions and unaffected ETS regions between WT and *Baf155* CKO YS EMPs (top panel). Also shown is ChIP-qPCR showing enrichment of PU.1 and BAF155 binding at selected myeloid gene loci (highlighted regions in the top panel, 1–6), negative control gene loci (highlighted regions in the top panel, 2n and 6n), and unaffected ETS regions (highlighted regions in the top panel, UER1 and UER2) in E10.5 WT YSs (bottom panel). qPCR primers and genomic locations are provided in Table S2. Data are presented as mean ± SD; n = 3.

(C) Cytoplasmic (Cyt) and nuclear (Nuc) protein input and anti-FLAG and isotype control (IgG1) immunoprecipitation of nuclear extracts from MEFs over-expressing FLAG-*Baf155* and *Pu.1*. Shown are immunoblots for BAF155, PU.1, BRG1, P300, and UTX (KDM6a).

(legend continued on next page)

line that expresses *Flag-Baf155* and *Pu.1* or *HA-Pu.1*. Cells were then subjected to immunoprecipitation using an antibody against the FLAG tag, followed by PU.1 or hemagglutinin (HA) immunoblot. PU.1 was co-immunoprecipitated with BAF155 (Figure 5C). Conversely, when the anti-HA antibody was used for immunoprecipitation, BAF155 was co-immunoprecipitated with PU.1 (Figure S5A). As reported previously (Alver et al., 2017; Narayanan et al., 2015), we additionally found BRG1, p300, and KDM6a (UTX) to be co-immunoprecipitated with BAF155, suggesting that PU.1 activates its target genes by forming a transcriptional complex with BAF, p300, and KDM6a. Because p300 and KDM6a mainly target H3K27, we postulated that PU.1 target gene loci remain methylated at H3K27 sites in the absence of BAF155, leading to repression of PU.1 target gene expression. Indeed, although inaccessible regions in *Baf155* CKO yolk sacs showed higher H3K27me3 levels compared with WT yolk sacs, H3K27me3 levels were similar at UER1 and UER2 in WT and CKO yolk sacs (Figure S5B). If this were truly the case, then we would expect that inhibition of EZH2, the catalytic subunit of Polycomb repressive complex 2 (PRC2), which methylates H3K27 (Laugesen et al., 2019), might rescue PU.1 target gene expression in *Baf155* CKO yolk sacs. Thus, we set up matings between *Tie2-Cre;Baf155*f/+ (father) and *Baf155*f/f (mother) mice and injected GSK-126 (an EZH2 inhibitor) intraperitoneally into the mother at E8. E9.5 yolk sacs were collected and subjected to qRT-PCR. Although vehicle treatment did not affect myeloid lineage gene expression, indicating that the GSK-126 effect would be specific (Figure S5C), expression of many PU.1 target genes was rescued in *Baf155* CKO yolk sacs when EZH2 was inhibited (Figure 5D). *Pu.1/Spi1* expression was also rescued, suggesting the BAF-mediated remodeling mechanism of PU.1 autoregulation. It is worth noting that GSK-126 treatment led to baseline elevation of expression of some genes, including *Irf8*, *Itgam*, *Gata2*, *Scl*, and *cKit* (Figures 5D and S5D), suggesting that these genes are normally repressed by the EZH2-mediated mechanism.

DISCUSSION

Chromatin remodeling by the mammalian BAF complex is required for the development of multiple lineages during embryogenesis. *Brg1* deletion within the Tie2(+) lineage leads to defective yolk sac angiogenesis and primitive erythropoiesis. EryP cell defects in these mice are due to increased apoptosis and lack of embryonic α- and β-globin gene expression (Griffin et al., 2008). We show that *Baf155* deletion within the Tie2(+) lineage also causes angiogenesis defects, as evidenced by hemorrhage in some *Baf155* CKO mice. However, we found that embryonic globin gene expression was similar, and EryPs and their progenitors were present at similar levels in WT and *Baf155* CKO yolk sacs. Unexpectedly, *Baf155* CKO mice display defective yolk sac myelopoiesis and definitive erythropoiesis. We attribute the phenotype difference between the two mice, *Tie2-Cre; Brg1*f/f and *Tie2-Cre; Baf155*f/f, to the nature of the deleted gene. *Brg1* encodes for an ATPase that is the core of the BAF complex, whereas *Baf155* encodes a BAF structural component. Presumably, *Baf155* deletion might have delayed the phenotype's manifestation to reflect the hematopoietic lineage hierarchy; i.e., the EC and EryP lineages arise before EMPs, which generate myeloid and EryD lineages. Intriguingly, we observed that EC genes were still expressed in *Baf155*-deficient EMPs, suggesting that the extinction of previous lineage genes is necessary for new lineage establishment. Alternatively, the previous lineage gene loci are still accessible in the absence of the next lineage gene loci's active chromatin remodeling. Collectively, these data establish that the BAF complex has a critical role in myeloid and EryD lineage differentiation from EMPs by remodeling the chromatin of the myeloid and EryD lineage gene loci.

Although chromatin remodeling is critical for developing many different lineages, it is still unclear whether and how the specificity of the BAF chromatin remodeling complex of the target genes is achieved. Our data demonstrate that BAF-mediated chromatin remodeling of myeloid and EryD lineage genes at the EMP stage is necessary for downstream myeloid and EryD lineage development. We found that DARs in WT and Baf155-deficient EMPs are enriched predominantly for the ETS motif. Moreover, BAF155 interacted with PU.1 and was recruited to PU.1 target gene loci. This strongly argues that the BAF complex's target gene specificity is achieved by ETS TFs. Consistent with this idea, recent studies have shown that AP-1 and ETS motifs are enriched in enhancer regions sensitive to *Smarcb1* loss (Alver et al., 2017). Moreover, TMPRSS2-ERG, a fusion gene product from a chromosomal translocation in prostate cancer, interacts with the BAF complex in an ETS-dependent manner (Sandoval et al., 2018), indicating that the BAF complex is required for ERG-mediated prostate oncogenesis. The BAF complex has been shown to interact with p300 and acetylates H3K27 (Alver et al., 2017). The BAF complex also interacts with KDM6a/6b and demethylates H3K27 (Narayanan et al., 2015). We also observed that BAF155 forms a complex with p300 and KDM6a. Our data show that DARs in *Baf155* CKO EMPs included mostly PU.1 target genes and displayed higher H3K27me3 levels. EZH2 inhibitor treatment could rescue some of the PU.1 target gene expression in *Baf155* CKO yolk sacs. These data suggest that PU.1 activates its target genes by forming a complex with BAF, p300, and KDM6a/6b and triggering H3K27 acetylation/demethylation of the target genes (Figure 5E). In the absence of the BAF complex, PU.1 target loci are occupied by EZH2, suppressing PU.1 target gene expression (Figure 5E).

(D) qRT-PCR analysis of *Cx3cr1*, *Irf8*, *Csf-1r*, *Pu.1/Spi1*, *Itgam*, and *Emr1* gene expression in E9.5 WT and *Baf155* CKO YSs with or without GSK126 treatment. Gene expression was normalized to the untreated WT mean value. Data are from at least four biological replicates for either genotype, with each replicate consisting of an individual YS. Data are presented as mean ± SD. Student's t test; *p < 0.05, **p < 0.01, ***p < 0.001.
(E) A model showing BAF-mediated chromatin remodeling in PU.1 transcriptional gene activation.
See also Figure S5.

Reduced *Pu.1* expression leads to acute myeloid leukemia (Will et al., 2015; Steidl et al., 2007). Moreover, *Pu.1* activation in hematopoietic stem and progenitor cells can lead to myeloid lineage skewing and deregulated hematopoiesis in chronic inflammatory conditions (Pietras et al., 2016; Etzrodt et al., 2019). Methylation of BAF155 at the R1064 residue by coactivator-associated arginine methyltransferase 1 (CARM1; also known as PRMT4) is critical for tumor progression and metastasis (Wang et al., 2014). Although CARM1 is essential for myeloid leukemogenesis, it is dispensable for normal hematopoiesis (Greenblatt et al., 2018). UTX (KDM6a) suppresses myeloid leukemogenesis partially by repressing an ETS-mediated transcriptional program (Gozdecka et al., 2018). *Kdm6b* is required for fetus-derived T-ALL and adult-derived AML (Mallaney et al., 2019). These studies collectively suggest that controlling *Pu.1* expression and its activity might be critical for managing cancer and chronic inflammatory diseases. Intriguingly, ETS factors can regulate *Baf155* expression (Ahn et al., 2005), supporting an interplay between ETS TFs and BAF expression and function. Future studies delineating the crosstalk between ETS factors and BAF and interaction among BAF, p300, PU.1, and KDM6a/6b and PU.1 target gene expression will be critical for further understanding myeloid lineage and leukemia development. Future applications of the epigenetics involving PU.1 and BAF155 expression and function for tissue repair, regeneration, and diseases are warranted.

STAR★METHODS

Detailed methods are provided in the online version of this paper and include the following:

- KEY RESOURCES TABLE
- RESOURCE AVAILABILITY
  - Lead Contact
  - Materials Availability
  - Data and Code Availability
- EXPERIMENTAL MODEL AND SUBJECT DETAILS
  - Mice
  - Cell culture and transduction
- METHOD DETAILS
  - Genotyping
  - Lentiviral and retroviral particle production
  - esiRNA transfection
  - Hematopoietic progenitor assays
  - *In vivo* GSK-126 treatment
  - Nuclear extract preparation
  - Immunoprecipitation
  - Western blotting
  - Chromatin immunoprecipitation (ChIP) coupled with quantitative real-time PCR (ChIP-qPCR)
  - Tissue processing for flow cytometry
  - Flow cytometry and cell sorting
  - Quantitative real-time reverse transcription PCR (qRT-PCR)
  - Single-cell RNA sequencing
  - ATAC-seq library generation, sequencing, and mapping

- QUANTIFICATION AND STATISTICAL ANALYSIS
  - scRNA-seq bioinformatics analyses
  - Identification of ATAC peaks
  - Identification and analyses of DARs
  - Statistics

AUTHOR CONTRIBUTIONS

J.W., K.K., and K.C. conceived and designed experiments and wrote the paper. J.W. and K.K. performed the experiments and analyzed the data. H.J.L. and X.X. performed and analyzed the ATAC-seq data. H.Z., S.P., and M.N.A. performed and analyzed the scRNA-seq data. R.H.S. provided the *Baf155^(f/f)* mice. X.W. and D.H.F. performed BAF155 and PU.1 immunoprecipitation and western blot analyses. S.P., H.J.L., M.N.A., and T.W. helped write the manuscript. K.C. provided overall supervision and coordinated all experimental activities.

REFERENCES

Ahn, J., Ko, M., Lee, K., Oh, J., Jeon, S.H., and Seong, R.H. (2005). Expression of SRG3, a core component of mouse SWI/SNF chromatin-remodeling complex, is regulated by cooperative interactions between Sp1/Sp3 and Ets transcription factors. Biochem. Biophys. Res. Commun. *338*, 1435–1446.

Alver, B.H., Kim, K.H., Lu, P., Wang, X., Manchester, H.E., Wang, W., Haswell, J.R., Park, P.J., and Roberts, C.W. (2017). The SWI/SNF chromatin remodelling complex is required for maintenance of lineage specific enhancers. Nat. Commun. *8*, 14648.

Azzoni, E., Frontera, V., McGrath, K.E., Harman, J., Carrelha, J., Nerlov, C., Palis, J., Jacobsen, S.E.W., and de Bruijn, M.F. (2018). Kit ligand has a critical role in mouse yolk sac and aorta-gonad-mesonephros hematopoiesis. EMBO Rep. *19*, e45477.

Buenrostro, J.D., Giresi, P.G., Zaba, L.C., Chang, H.Y., and Greenleaf, W.J. (2013). Transposition of native chromatin for fast and sensitive epigenomic profiling of open chromatin, DNA-binding proteins and nucleosome position. Nat. Methods *10*, 1213–1218.

Bultman, S., Gebuhr, T., Yee, D., La Mantia, C., Nicholson, J., Gilliam, A., Randazzo, F., Metzger, D., Chambon, P., Crabtree, G., and Magnuson, T. (2000). A Brg1 null mutation in the mouse reveals functional differences among mammalian SWI/SNF complexes. Mol. Cell *6*, 1287–1295.

Butler, A., Hoffman, P., Smibert, P., Papalexi, E., and Satija, R. (2018). Integrating single-cell transcriptomic data across different conditions, technologies, and species. Nat. Biotechnol. *36*, 411–420.

Chen, H., Ray-Gallet, D., Zhang, P., Hetherington, C.J., Gonzalez, D.A., Zhang, D.E., Moreau-Gachelin, F., and Tenen, D.G. (1995). PU.1 (Spi-1) autoregulates its expression in myeloid cells. Oncogene 11, 1549–1560.

Chen, M.J., Li, Y., De Obaldia, M.E., Yang, Q., Yzaguirre, A.D., Yamada-Inagawa, T., Vink, C.S., Bhandoola, A., Dzierzak, E., and Speck, N.A. (2011). Erythroid/myeloid progenitors and hematopoietic stem cells originate from distinct populations of endothelial cells. Cell Stem Cell 9, 541–552.

Choi, J., Ko, M., Jeon, S., Jeon, Y., Park, K., Lee, C., Lee, H., and Seong, R.H. (2012). The SWI/SNF-like BAF complex is essential for early B cell development. J. Immunol. 188, 3791–3803.

Corces, M.R., Trevino, A.E., Hamilton, E.G., Greenside, P.G., Sinnott-Armstrong, N.A., Vesuna, S., Satpathy, A.T., Rubin, A.J., Montine, K.S., Wu, B., et al. (2017). An improved ATAC-seq protocol reduces background and enables interrogation of frozen tissues. Nat. Methods 14, 959–962.

Etzrodt, M., Ahmed, N., Hoppe, P.S., Loeffler, D., Skylaki, S., Hilsenbeck, O., Kokkaliaris, K.D., Kaltenbach, H.M., Stelling, J., Nerlov, C., and Schroeder, T. (2019). Inflammatory signals directly instruct PU.1 in HSCs via TNF. Blood 133, 816–819.

Ginhoux, F., Greter, M., Leboeuf, M., Nandi, S., See, P., Gokhan, S., Mehler, M.F., Conway, S.J., Ng, L.G., Stanley, E.R., et al. (2010). Fate mapping analysis reveals that adult microglia derive from primitive macrophages. Science 330, 841–845.

Gomez Perdiguero, E., Klapproth, K., Schulz, C., Busch, K., Azzoni, E., Crozet, L., Garner, H., Trouillet, C., de Bruijn, M.F., Geissmann, F., and Rodewald, H.R. (2015). Tissue-resident macrophages originate from yolk-sac-derived erythro-myeloid progenitors. Nature 518, 547–551.

Gozdecka, M., Meduri, E., Mazan, M., Tzelepis, K., Dudek, M., Knights, A.J., Pardo, M., Yu, L., Choudhary, J.S., Metzakopian, E., et al. (2018). UTX-mediated enhancer and chromatin remodeling suppresses myeloid leukemogenesis through noncatalytic inverse regulation of ETS and GATA programs. Nat. Genet. 50, 883–894.

Greenblatt, S.M., Man, N., Hamard, P.J., Asai, T., Karl, D., Martinez, C., Bilbao, D., Stathias, V., Jermakowicz, A.M., Duffort, S., et al. (2018). CARM1 Is Essential for Myeloid Leukemogenesis but Dispensable for Normal Hematopoiesis. Cancer Cell 33, 1111–1127.e5.

Griffin, C.T., Brennan, J., and Magnuson, T. (2008). The chromatin-remodeling enzyme BRG1 plays an essential role in primitive erythropoiesis and vascular development. Development 135, 493–500.

Han, D., Jeon, S., Sohn, D.H., Lee, C., Ahn, S., Kim, W.K., Chung, H., and Seong, R.H. (2008). SRG3, a core component of mouse SWI/SNF complex, is essential for extra-embryonic vascular development. Dev. Biol. 315, 136–146.

Hargreaves, D.C., and Crabtree, G.R. (2011). ATP-dependent chromatin remodeling: genetics, genomics and mechanisms. Cell Res. 21, 396–420.

Hashimoto, D., Chow, A., Noizat, C., Teo, P., Beasley, M.B., Leboeuf, M., Becker, C.D., See, P., Price, J., Lucas, D., et al. (2013). Tissue-resident macrophages self-maintain locally throughout adult life with minimal contribution from circulating monocytes. Immunity 38, 792–804.

Heinz, S., Benner, C., Spann, N., Bertolino, E., Lin, Y.C., Laslo, P., Cheng, J.X., Murre, C., Singh, H., and Glass, C.K. (2010). Simple combinations of lineage-determining transcription factors prime cis-regulatory elements required for macrophage and B cell identities. Mol. Cell 38, 576–589.

Hoeffel, G., and Ginhoux, F. (2018). Fetal monocytes and the origins of tissue-resident macrophages. Cell. Immunol. 330, 5–15.

Kadoch, C., and Crabtree, G.R. (2015). Mammalian SWI/SNF chromatin remodeling complexes and cancer: Mechanistic insights gained from human genomics. Sci. Adv. 1, e1500447.

Kim, J.K., Huh, S.O., Choi, H., Lee, K.S., Shin, D., Lee, C., Nam, J.S., Kim, H., Chung, H., Lee, H.W., et al. (2001). Srg3, a mouse homolog of yeast SWI3, is essential for early embryogenesis and involved in brain development. Mol. Cell. Biol. 21, 7787–7795.

Langmead, B., and Salzberg, S.L. (2012). Fast gapped-read alignment with Bowtie 2. Nat. Methods 9, 357–359.

Laugesen, A., Højfeldt, J.W., and Helin, K. (2019). Molecular Mechanisms Directing PRC2 Recruitment and H3K27 Methylation. Mol. Cell 74, 8–18.

Lickert, H., Takeuchi, J.K., Von Both, I., Walls, J.R., McAuliffe, F., Adamson, S.L., Henkelman, R.M., Wrana, J.L., Rossant, J., and Bruneau, B.G. (2004). Baf60c is essential for function of BAF chromatin remodelling complexes in heart development. Nature 432, 107–112.

Lybarger, L., Wang, X., Harris, M.R., Virgin, H.W., 4th, and Hansen, T.H. (2003). Virus subversion of the MHC class I peptide-loading complex. Immunity 18, 121–130.

Mallaney, C., Ostrander, E.L., Celik, H., Kramer, A.C., Martens, A., Kothari, A., Koh, W.K., Haussler, E., Iwamori, N., Gontarz, P., et al. (2019). Kdm6b regulates context-dependent hematopoietic stem cell self-renewal and leukemogenesis. Leukemia 33, 2506–2521.

Martin, M. (2011). Cutadapt removes adapter sequences from high-throughput sequencing reads. EMBnet. J. 17, 10–12.

McGrath, K.E., Frame, J.M., Fegan, K.H., Bowen, J.R., Conway, S.J., Catherman, S.C., Kingsley, P.D., Koniski, A.D., and Palis, J. (2015). Distinct Sources of Hematopoietic Progenitors Emerge before HSCs and Provide Functional Blood Cells in the Mammalian Embryo. Cell Rep. 11, 1892–1904.

McLean, C.Y., Bristor, D., Hiller, M., Clarke, S.L., Schaar, B.T., Lowe, C.B., Wenger, A.M., and Bejerano, G. (2010). GREAT improves functional interpretation of cis-regulatory regions. Nat. Biotechnol. 28, 495–501.

Narayanan, R., Pirouz, M., Kerimoglu, C., Pham, L., Wagener, R.J., Kiszka, K.A., Rosenbusch, J., Seong, R.H., Kessel, M., Fischer, A., et al. (2015). Loss of BAF (mSWI/SNF) Complexes Causes Global Transcriptional and Chromatin State Changes in Forebrain Development. Cell Rep. 13, 1842–1854.

Palis, J. (2016). Hematopoietic stem cell-independent hematopoiesis: emergence of erythroid, megakaryocyte, and myeloid potential in the mammalian embryo. FEBS Lett. 590, 3965–3974.

Pietras, E.M., Mirantes-Barbeito, C., Fong, S., Loeffler, D., Kovtonyuk, L.V., Zhang, S., Lakshminarasimhan, R., Chin, C.P., Techner, J.M., Will, B., et al. (2016). Chronic interleukin-1 exposure drives haematopoietic stem cells towards precocious myeloid differentiation at the expense of self-renewal. Nat. Cell Biol. 18, 607–618.

Ramírez, F., Ryan, D.P., Grüning, B., Bhardwaj, V., Kilpert, F., Richter, A.S., Heyne, S., Dündar, F., and Manke, T. (2016). deepTools2: a next generation web server for deep-sequencing data analysis. Nucleic Acids Res. 44 (W1), W160-5.

Ross-Innes, C.S., Stark, R., Teschendorff, A.E., Holmes, K.A., Ali, H.R., Dunning, M.J., Brown, G.D., Gojis, O., Ellis, I.O., Green, A.R., et al. (2012). Differential oestrogen receptor binding is associated with clinical outcome in breast cancer. Nature 481, 389–393.

Sandoval, G.J., Pulice, J.L., Pakula, H., Schenone, M., Takeda, D.Y., Pop, M., Boulay, G., Williamson, K.E., McBride, M.J., Pan, J., et al. (2018). Binding of TMPRSS2-ERG to BAF Chromatin Remodeling Complexes Mediates Prostate Oncogenesis. Mol. Cell 71, 554–566.e7.

Schulz, C., Gomez Perdiguero, E., Chorro, L., Szabo-Rogers, H., Cagnard, N., Kierdorf, K., Prinz, M., Wu, B., Jacobsen, S.E., Pollard, J.W., et al. (2012). A lineage of myeloid cells independent of Myb and hematopoietic stem cells. Science 336, 86–90.

Steidl, U., Steidl, C., Ebralidze, A., Chapuy, B., Han, H.J., Will, B., Rosenbauer, F., Becker, A., Wagner, K., Koschmieder, S., et al. (2007). A distal single nucleotide polymorphism alters long-range regulation of the PU.1 gene in acute myeloid leukemia. J. Clin. Invest. 117, 2611–2620.

Takeuchi, J.K., and Bruneau, B.G. (2009). Directed transdifferentiation of mouse mesoderm to heart tissue by defined factors. Nature 459, 708–711.

Tober, J., Koniski, A., McGrath, K.E., Vemishetti, R., Emerson, R., de Mesy-Bentley, K.K., Waugh, R., and Palis, J. (2007). The megakaryocyte lineage originates from hemangioblast precursors and is an integral component both of primitive and of definitive hematopoiesis. Blood 109, 1433–1441.

Wang, L., Zhao, Z., Meyer, M.B., Saha, S., Yu, M., Guo, A., Wisinski, K.B., Huang, W., Cai, W., Pike, J.W., et al. (2014). CARM1 methylates chromatin

remodeling factor BAF155 to enhance tumor progression and metastasis. Cancer Cell *25*, 21–36.

Will, B., Vogler, T.O., Narayanagari, S., Bartholdy, B., Todorova, T.I., da Silva Ferreira, M., Chen, J., Yu, Y., Mayer, J., Barreyro, L., et al. (2015). Minimal PU.1 reduction induces a preleukemic state and promotes development of acute myeloid leukemia. Nat. Med. *21*, 1172–1181.

Wu, J.I., Lessard, J., and Crabtree, G.R. (2009). Understanding the words of chromatin regulation. Cell *136*, 200–206.

Zhang, Y., Liu, T., Meyer, C.A., Eeckhoute, J., Johnson, D.S., Bernstein, B.E., Nusbaum, C., Myers, R.M., Brown, M., Li, W., and Liu, X.S. (2008). Model-based analysis of ChIP-Seq (MACS). Genome Biol. *9*, R137.

Zhao, H., and Choi, K. (2019). Single cell transcriptome dynamics from pluripotency to FLK1$^+$ mesoderm. Development *146*, dev182097.

Zhou, X., Maricque, B., Xie, M., Li, D., Sundaram, V., Martin, E.A., Koebbe, B.C., Nielsen, C., Hirst, M., Farnham, P., et al. (2011). The Human Epigenome Browser at Washington University. Nat. Methods *8*, 989–990.

STAR★METHODS

KEY RESOURCES TABLE

REAGENT or RESOURCE	SOURCE	IDENTIFIER
Antibodies		
Anti-mouse CDD45-BV421 (Clone 30-F11)	BioLegend	Cat#103134; RRID:AB_2562559
Anti-mouse CDD45-APC (Clone 30-F11)	BioLegend	Cat#103112; RRID:AB_312977
Anti-mouse TER119-PE (Clone TER-119)	BioLegend	Cat#116208; RRID:AB_313709
Anti-mouse TER119-APC-Cy7 (Clone TER-119)	BioLegend	Cat#116223; RRID:AB_2137788
Anti-mouse CD31-Biotin (Clone MEC13.3)	BioLegend	Cat#102504; RRID:AB_312911
Anti-mouse CD31-FITC (Clone MEC13.3)	BD Biosciences	Cat#553372; RRID:AB_394818
Anti-mouse/human CD11b-BV421 (Clone M1/70)	BioLegend	Cat#101235; RRID:AB_10897942
Anti-mouse/human CD11b-Biotin (Clone M1/70)	BioLegend	Cat#101204; RRID:AB_312787
Anti-mouse F4/80-PE (Clone BM8)	BioLegend	Cat#123110; RRID:AB_893486
Anti-mouse F4/80-APC (Clone BM8)	BioLegend	Cat#123116; RRID:AB_893481
Anti-mouse CX3CR1-PE (Clone SA011F11)	BioLegend	Cat#149006; RRID:AB_2564315
Anti-mouse CD117(c-Kit)-PE (Clone 2B8)	BioLegend	Cat#105807; RRID:AB_313216
Anti-mouse CD117(c-Kit)-APC (Clone 2B8)	BioLegend	Cat#105812; RRID:AB_313221
Anti-mouse CD41-APC (Clone MWReg30)	BioLegend	Cat#133914; RRID:AB_11125581
Anti-mouse CD16/32-BV421 (Clone 93)	BioLegend	Cat#101331; RRID:AB_2562188
Anti-mouse CD16/32-PE (Clone 2.4G2)	BD Biosciences	Cat#553145; RRID:AB_394660
Purified anti-mouse CD16/32 (Clone 93)	BioLegend	Cat# 101302; RRID:AB_312801
BV421-Streptavidin	BioLegend	Cat#405225 (No RRID number available)
BV605-Streptavidin	BD Biosciences	Cat#563260 (No RRID number available)
SMARCC1/BAF155 (D7F8S) Rabbit mAb antibody	Cell Signaling Tech.	Cat#11956; RRID:AB_2797776
PU.1 (9G7) Rabbit mAb antibody	Cell Signaling Tech.	Cat# 2258; RRID:AB_2186909
p300 (D8Z4E) Rabbit mAb antibody	Cell Signaling Tech.	Cat# 86377; RRID:AB_2800077
Brg1 (D1Q7F) Rabbit mAb antibody	Cell Signaling Tech.	Cat# 49360; RRID:AB_2728743
UTX (D3Q1I) Rabbit mAb antibody	Cell Signaling Tech.	Cat# 33510; RRID:AB_2721244
HA-Tag(C29F4) Rabbit mAb antibody	Cell Signaling Tech.	Cat# 3724; RRID:AB_1549585
Rabbit IgG	Cell Signaling Tech.	Cat#2729; RRID:AB_1031062
Rabbit Anti-Histone H3, trimethyl (Lys27) Polyclonal antibody	Millipore	Cat# 07-449; RRID:AB_310624
Monoclonal ANTI-FLAG® M2 antibody	Sigma-Aldrich	Cat# F3165; RRID:AB_259529
EZview Red ANTI-FLAG® M2 Affinity Gel	Sigma-Aldrich	Cat# F2426; RRID:AB_2616449
EZview Red Anti-HA Affinity Gel	Sigma-Aldrich	Cat# E6779; RRID:AB_10109562
Bacterial and Virus Strains		
One Shot Stbl3 Chemically Competent E.Coli	Thermo Fisher Scientific	Cat#C737303
Chemicals, Peptides, and Recombinant Proteins		
DMEM	GIBCO	Cat#11965092
FBS	Atlanta Biologicals	Cat#S12450
L-Glutamine	GIBCO	Cat#35050061
MEM Non-Essential Amino Acids	Corning	Cat#25-025-CI
MEM Sodium Pyruvate	Corning	Cat#25-000-CI
Geneticin	GIBCO	Cat#10131-035

(Continued on next page)

Continued

REAGENT or RESOURCE	SOURCE	IDENTIFIER
Puromycin	Sigma	Cat#P8833
Blasticidin S Hydrochloride	Research Products International Corp	Cat#B12200
penicillin-streptomycin	GIBCO	Cat# 15140122
IMDM	GIBCO	Cat#2440046
Hexadimethrine bromide	Sigma	Cat#H9268
Interleukin-3 (IL-3) supernatant	This paper	N/A
Murine stem cell factor	PeproTech	Cat#250-03
M-CSF	PeproTech	Cat#315-02
GM-CSF	PeproTech	Cat#315-03
IL-6	PeproTech	Cat#216-16
IL-11	R&D Systems	Cat#418-ML
Erythropoietin (EPO)	PeproTech	Cat#100-64
Lipofectamine 3000	Thermo Fisher Scientific	Cat#L3000-001
esiBaf155	Sigma	Cat#EMU012611-50UG
esiEGFP	Sigma	Cat#EHUEGFP-50UG
MethoCult3434	Stem Cell Technologies	Cat#M3434
GSK-126	MedChem	Cat#HY-13470
SBE-β-CD	MedChem	Cat# HY-17031
DSP (Dithiobis (succinimidyl propionate))	Thermo Fisher Scientific	Cat#22585
0.25% trypsin-EDTA	GIBCO	Cat#25200-056
Protease inhibitor cocktail	Sigma	Cat#11836170001
Tween 20	Sigma	Cat#P9416
Iodoacetamide	Sigma	Cat#I6125
Sepharose 4B	Sigma	Cat#4B200
LDS buffer	Invitrogen	Cat#NP0007
Beta – mercaptoethanol	Sigma	Cat#444203
ECL chemiluminescence substrate	Thermo Fisher Scientific	Cat#32106
Collagenase type IV	Worthington	Cat#LS004188
Deoxyribonuclease I	Worthington	Cat#LS002139
0.25% Collagenase	Stem Cell Technologies	Cat#07902
ProteinA-Sepharose® 4	Sigma-Aldrich	Cat#P9424
Critical Commercial Assays		
QuickTiter Lentivirus Associated HIV p24 Titer Kit	Cell Biolabs, INC	Cat#VPK-107
SimpleChIP® Plus Enzymatic Chromatin IP Kit	Cell Signaling Tech.	Cat#9005
RNeasy Micro/Mini Kit	QIAGEN	Cat#74004/74106
qScript cDNA SuperMix	Quanta	Cat#101414-106
DNA Clean and Concentrator 5	Zymo Research	Cat#D4014
AMPure XP beads	Beckman Coulter	N/A
Deposited Data		
ATAC-seq data	This paper	GEO: GSE144243
GRCm10/mm10	UCSC genome browser	http://hgdownload.soe.ucsc.edu/goldenPath/mm10/bigZips/
scRNA-seq data	This paper	GEO: GSE159381
scRNA-seq data of WT cells	Zhao and Choi, 2019	GEO: GSE130146
Experimental Models: Cell Lines		
293FT cell line	ThermoFisher	Cat#R70007

Continued

REAGENT or RESOURCE	SOURCE	IDENTIFIER
Platinum-E (Plat-E) retroviral packaging cell line	Cell Biolabs, INC	Cat#RV-101
Mouse Embryonic Fibroblast (MEF)	Hansen, T.H. Washington University in St. Louis; Lybarger et al., 2003	N/A
MEF-Flag-Baf155-IRES-GFP+Pu.1-IRES-mCherry	This paper	N/A
MEF-Flag-Baf155+HA-PU.1	This paper	N/A
Experimental Models: Organisms/Strains		
C57Bl6/J Wild Type	Jackson Laboratories	Stock No:000664
Tie2-Cre	Jackson Laboratories	Stock No:004128
Baf155^f/f	Rho Hyun Seong; Choi et al., 2012	N/A
Oligonucleotides		
See Tables S2 and S3 for a list of oligonucleotide sequences		N/A
Recombinant DNA		
pRRL_CAGpN-Flag-Baf155-IRES-GFP	Addgene	Cat#24561; RRID:Addgene_24561
CSII-EF-MCS-IRES2-bsr-PU.1-HA	This paper	N/A
psPAX2	Addgene	Cat#12260; RRID:Addgene_12260
pMD2.G	Addgene	Cat#12259; RRID:Addgene_12259
Pu.1-IRES-mCherry retroviral plasmid DNA	Addgene	Cat#80140; RRID:Addgene_80140
pLKO.1-puro-Ubc-TurboGFP	Sigma	Cat#SHC014; (No RRID number available)
Software and Algorithms		
FlowJo software version 10.5.3	TreeStar Inc.	https://www.flowjo.com
Graphpad Prism version 8.4.3	Graphpad Software, LLC.	https://www.graphpad.com/scientific-software/prism/
Cutadapt version 1.11	Martin, 2011	https://github.com/marcelm/cutadapt/
Bowtie 2 version 2.3.4.1	Langmead and Salzberg, 2012	http://bowtie-bio.sourceforge.net/bowtie2/index.shtml
MACS2 version 2.1.1	Zhang et al., 2008	https://github.com/macs3-project/MACS
WashU Epigenome Browser	Zhou et al., 2011	https://epigenomegateway.wustl.edu/
DiffBind version 2.6.6	Ross-Innes et al., 2012	https://bioconductor.org/packages/release/bioc/html/DiffBind.html
deepTools	Ramírez et al., 2016	https://github.com/deeptools/deepTools
GREAT version 4.0.4	McLean et al., 2010	http://great.stanford.edu/public/html/index.php
HOMER version 4.8	Heinz et al., 2010	http://homer.ucsd.edu/homer/index.html
Cell Ranger Single Cell Software Suite (v2.0.1)	Cell Ranger	https://support.10xgenomics.com/single-cell-gene-expression/software/pipelines/latest/what-is-cell-ranger
Seurat version 2.3.4	Seurat	https://satijalab.org/seurat/
Other		
Fisherbrand Model 120 Sonic Dismembrator	Fisher scientific	N/A

RESOURCE AVAILABILITY

Lead Contact

Further information and requests for resources and reagents should be directed to and will be fulfilled by the corresponding author and Lead Contact, Dr. Kyunghee Choi (kchoi@wustl.edu).

Materials Availability
This study did not generate any unique reagents.

Data and Code Availability
The ATAC-seq data discussed in this publication have been deposited in NCBI's Gene Expression Omnibus and are accessible through GEO Series accession number GSE144243 (https://www.ncbi.nlm.nih.gov/geo/query/acc.cgi?acc=GSE144243).

The accession number for the scRNA-Seq data reported in this paper is GEO: GSE159381.

EXPERIMENTAL MODEL AND SUBJECT DETAILS

Mice
Tie2-Cre;Baf155 CKO mice were obtained by first crossing *Tie2-Cre* (Stock No: 4128, Jackson Labs) males (2-3 months old) to *Baf155*$^{f/f}$ (Choi et al., 2012) females (2-3 months old) to generate *Tie2*-cre; *Baf155*$^{f/+}$ mice. Next, timed matings using *Tie2-Cre*; *Baf155*$^{f/+}$ males (2-8 months old) and *Baf155*$^{f/f}$ females (2-3 months old) were set up in the evening and females checked for vaginal plugs the following morning (12pm = E0.5). Females were separated from males and housed in the animal barrier until the desired time point. Females were euthanized using CO_2 asphyxiation and uteri removed for embryo collection. Embryos and collected tissue were kept on ice in PBS with 10% FBS until processed for analysis. Wild-type (WT) littermates were used as controls. Animal husbandry, generation, and handling were performed in accordance with protocols approved by the Institutional Animal Care and Use Committee of Washington University School of Medicine in St. Louis.

Cell culture and transduction
The Mouse Embryonic Fibroblast (MEF) cell line has been previously described (Lybarger et al., 2003). MEF and MEF-derived stable cell lines were cultured in Iscove's Modified Dulbecco's Medium (IMDM) (2440046, GIBCO) supplemented with 10% (v/v) Fetal bovine serum (FBS) (S12450, Atlanta Biologicals), and 100U/ml penicillin-streptomycin (15140122, GIBCO). MEF cells were transduced with Flag-*Baf155*-IRES-GFP lentiviral and *Pu.1*-IRES-mCherry retroviral particles. Hexadimethrine bromide (8 μg/ml) (H9268, Sigma) was added during transductions to increase viral particle uptake. Transduced cells were sorted twice to ensure greater than 90% purity. When HA-*Pu.1* lentivirus was used, MEF-Flag-*Baf155* cells were transduced with HA-*Pu.1* lentiviral particles and selected with 1μg/ml Blasticidin S Hydrochloride for 2 weeks. The overexpression efficiency of target proteins was confirmed by western blot.

METHOD DETAILS

Genotyping
The following primers were used to obtain genotype information for breeders and embryos:

Baf155 - TGTCATCCATGAGGAGTGGTC3′ (F); 5′GGTAGCTCACAAATGCCTGT3′ (R); WT = 400 bp; Floxed = 450 bp. Cre - 5′ACCAGAGACGGAAATCCATCG3′ (F); 5′CCACGACCA AGTGACAGCAATG3′ (R); Cre = 390 bp.

Lentiviral and retroviral particle production
Baf155 lentiviral plasmid DNA, pRRL_CAGpN-Flag-*Baf155*-IRES-GFP, was a gift from Jerry Crabtree (Addgene, plasmid# 2456). MISSION pLKO.1-puro-Ubc-TurboGFP (Sigma, SHC014) was used as a transduction efficiency control. The *Pu.1* lentiviral plasmid was constructed by adding a HA tag at the *Pu.1* N-terminal and inserting it into the CSII-EF-MCS-IRES2-bsr lentiviral backbone. Lentiviral packaging plasmid psPAX2 (Addgene, plasmid# 12260) and VSV-G envelope expressing plasmid pMD2.G (Addgene, plasmid# 12259) were gifts from Didier Trono. For cloning purposes, viral plasmid DNA was transformed using One Shot Stbl3 Chemically Competent E.Coli (C737303, ThermoFisher). Lentiviral particles were produced using the 293FT cell line (R70007, ThermoFisher), which was maintained in high glucose Dulbecco's Modified Eagle Medium (DMEM) (11965092, GIBCO), 10% FBS, 200 mM L-Glutamine (35050061, GIBCO), 10 mM MEM Non-Essential Amino Acids (25-025-Cl, Corning), 100 mM MEM Sodium Pyruvate (25-000-Cl, Corning), and 500 μg/ml Geneticin (10131-035, GIBCO). Cells were transfected with lentiviral DNA using the calcium phosphate method. Sixteen hours after transfection, media was replaced and cells were incubated at 37°C in 5% CO_2 for an additional 48 hours. Virus titer was determined by QuickTiter Lentivirus Associated HIV p24 Titer Kit (Cell Biolabs, INC). *Pu.1*-IRES-mCherry retroviral plasmid DNA was a gift from Ellen Rothenberg (Addgene, plasmid# 80140). Platinum-E (Plat-E) retroviral packaging cell line was used to generate the *Pu.1* retrovirus using the calcium phosphate method. Cells were maintained in high glucose DMEM supplemented with 10% FBS, 1 μg/ml puromycin (P8833, Sigma), 10 μg/ml Blasticidin S Hydrochloride (B12200, Research Products International Corp), and 100 U/ml penicillin-streptomycin. Media was replaced the following morning and virus harvested 48 hours after transfection.

esiRNA transfection
E10.5 WT yolk sac (YS) cKIT$^+$ cells (1x10^4) were plated in 100 μL maturation media (IMDM, 20% FBS, 1% interleukin-3 (IL-3) supernatant, 10 ng/ml murine stem cell factor (PeproTech), 10 ng/ml M-CSF (PeproTech), 10 ng/ml GM-CSF (PeproTech), 10 ng/ml IL-6,

10 ng/ml IL-11 (R&D Systems) and 2 U/ml erythropoietin (PeproTech) in a 96-well plate and transfected with 300 ng esiRNA against either *Baf155* (Sigma, EMU012611) or *Egfp* (Sigma, EHUEGFP) with 2 μL lipofectamine 3000 (Thermofisher). Cells were cultured in a 37°C incubator with 5% CO_2 for 36-48 hours and then subjected to either RNA extraction or re-plating in methylcellulose (MethoCult 3434, Stem Cell Technologies).

Hematopoietic progenitor assays
Methylcellulose colony-forming assays were performed using MethoCult 3434 (Stem Cell Technologies). E10.5 WT YS were pooled and sorted for either cKIT$^+$ or cKIT$^+$CD41$^+$CD16/32$^+$ populations. Sorted cells were mixed in methylcellulose (2,000 /ml) and plated in triplicate using 35mm Petri-dishes. Cultures were maintained in a humidified incubator at 37°C, 5% CO_2. CFU-E colonies were counted after 2-3 days of culture. Primitive erythroid, definitive erythroid (BFU-E), macrophage, and granulocyte/macrophage colonies were counted following 5-7 days of culture.

In vivo GSK-126 treatment
GSK-126 (HY-13470, MedChem) was dissolved in SBE-β-CD (HY-17031, MedChem) at a final concentration of 20 mg/ml. Pregnant mice (E8) were injected intraperitoneally with equal volumes of either SBE-β-CD (vehicle) or GSK126 (100mg/kg). At E9.5, pregnant females were euthanized using CO_2 asphyxiation and the uteri removed for embryo collection and dissection.

Nuclear extract preparation
Transduced MEF cells expressing *Baf155* and *Pu.1* were treated with DSP (Dithiobis [succinimidyl propionate], Thermo Scientific), a membrane permeable cleavable crosslinker, before subjected to nuclear extraction. Cells were detached using 0.25% trypsin-EDTA, washed twice with phosphate-buffered saline (PBS), resuspended in PBS containing 1mM DSP at approximately 1x10^7/ml, and incubated at room temperature (RT) for 30 min. The crosslink reaction was stopped by adding 1M Tris-HCl (pH7.5) at a final concentration of 20mM for 10min. DSP treated cells after wash were then incubated in hypotonic buffer (25mM HEPES (pH7.6), 25mM KCl, 5mM MgCl2, 0.05mM EDTA, 0.1% NP40, 5% Glycerol, 1mM PMSF) on ice for 10min, vigorously vortexed for 10 s, and centrifuged at 13,000 xg for 1 min. Supernatant, primarily containing soluble cytosolic protein, was collected for immunoblot while the pellet containing nuclei was resuspended in nuclear extraction buffer (10mM HEPES (pH7.6), 100mM KCl, 3mM MgCl$_2$, 0.1mM EDTA, 5% Glycerol supplemented with 1mM PMSF and 1X protease inhibitor cocktail (complete mini Roche, 11836170001, Sigma)), incubated on ice for 15min, and followed by 3x10s of sonication at 50% amplitude. Insoluble proteins and debris were removed from the nuclear extract by high-speed centrifugation (10 min at 18,000 g).

Immunoprecipitation
Nuclear extract was mixed 1:1 with IP buffer (10 mM Tris-HCl (pH 7.5), 200 mM NaCl, 1 mM EDTA, 0.2% Tween 20, 1X protease inhibitor cocktail, 20mM Iodoacetamide) and precleared by Sepharose 4B (4B200, Sigma). Immunoprecipitation was performed by incubating precleared nuclear extract with antibody-bound beads (anti-Flag M2 affinity gel, anti-HA (clone HA-7) affinity gel, or Protein A as a negative control (Sigma)) at 4°C overnight. Precipitates were washed 4 times with washing buffer (10 mM Tris-HCl (pH 7.5), 150 mM NaCl, 0.1% Tween 20, 20 mM Iodoacetamide) and eluted in 1X LDS buffer (Invitrogen). DSP was cleaved by adding 5% beta- mercaptoethanol in LDS loading buffer at 100°C for 10 min.

Western blotting
Western blotting was conducted following standard protocols. Primary antibodies used for western blotting are listed in key resources table. Secondary antibodies were horseradish peroxidase-conjugated mouse anti-rabbit IgG light chain and mouse IgG kappa chain binding protein (Santa Cruz Biotechnology, 1:10,000 dilution). Membranes were developed with ECL chemiluminescence substrate (ThermoFisher) and visualized using photographic film.

Chromatin immunoprecipitation (ChIP) coupled with quantitative real-time PCR (ChIP-qPCR)
Chromatin immunoprecipitation (ChIP) was performed according to the manufacture's protocol (ChIP kit, 9005, Cell Signaling Technologies) with the following modification: 25 mg cross-linked YS tissue was used per preparation. After cell lysis, nuclei extracts were digested by adding 0.5 μL Micrococcal Nuclease per IP prep and incubating for 20 min at 37°C with frequent mixing to digest DNA to a size of approximately 150-900 bp. Digestion was stopped by adding 10 μL 0.5 M EDTA and samples placed on ice for 2 min. Nuclei was pelleted and resuspend in 100 μL ChIP buffer. Nuclear lysates were further subjected to sonication to break nuclear membrane using a 120 Sonic Dismembrator (Fisher Scientific) at 4°C for 3 cycles, cycling ON for 10 s and OFF for 30 s at 50% amplitude. Approximately 10 μg of digested, cross-linked chromatin and 5 μg of antibody (BAF155, Cell Signaling Technologies, 11956; PU.1, Cell Signaling Technologies, 2258; H3K27me3, Millipore,07-449) were used per immunoprecipitation. IP samples were incubated overnight at 4°C with rotation, followed by 30 μL of protein G Magnetic Beads per IP reaction, and incubated for an additional 2 hr at 4°C with rotation. After elution of chromatin from the antibody/protein G magnetic beads, reverse cross-link performed by adding 6 μL 5 M NaCl and 2 μL proteinase K per IP, and incubating for 6 hr at 65°C. Immunoprecipitated DNA fragments were isolated using spin

columns provided by the kit and subjected to qPCR with appropriate primers indicated in Table S2. Rabbit IgG (Cell Signaling Technologies, 2729) was used as a negative control. Quantitative PCR was performed in triplicate from 3 independent experiments, and data were normalized to input values.

Tissue processing for flow cytometry

YS were collected between E8.25-10.5, and brain rudiments collected between E9.5-10.5. To obtain single-cell suspension, tissues were incubated in Hank's balanced salt solution (HBSS) containing 0.2 mg/ml collagenase type IV (Worthington), 100 U/ml deoxyribonuclease I (Worthington) and 5% FBS at 37°C for 1 h with tubes inverted every 5 to 10 min. Tissues were further dissociated by gently passing through a 20G needle 5 to 10 times. Cells were pelleted and resuspend in 0.3-1 mL IMDM media with 10% FBS. Cells were then passed through a 70 μm cell strainer and counted for viability.

Flow cytometry and cell sorting

Single cell suspensions were centrifuged at 400 g for 5 min, resuspended in 200 μL staining buffer (1X PBS, 1% BAS, 2 mM EDTA), placed in 5ml round-bottom tubes, and immunolabeled for FACS analysis. Before immunostaining, cell suspensions were pre-incubated with diluted (1:50) purified anti-CD16/32 (clone: 93, Biolegend, 101302) for 10 min on ice to block non-specific binding to Fc-receptors. Next, antibodies were added and incubated for 40 min on ice. Where appropriate, cells were further incubated with streptavidin conjugates for 20 min. All antibodies used can be found in key resources table. All FACS analyses were carried out on LSR Fortessa or Fortessa X-20 (BD Biosciences). Cell sorting was performed on FACS Aria II (BD Biosciences) sorter using 85 μm nozzle. All data were analyzed using FlowJo10 software (Tree Star).

Quantitative real-time reverse transcription PCR (qRT-PCR)

Total RNA from YS was prepared with RNeasy Micro/Mini Kit (QIAGEN), and reverse-transcribed into cDNA with qScript cDNA SuperMix (101414-106, Quanta) according to the manufacturer's protocol. Gene expression was measured by quantitative real-time PCR with primers indicated in Table S3. Gene expression levels were normalized to β-actin.

Single-cell RNA sequencing

An equal number of E9.5 and E10.5 WT YS were combined and dissociated with 0.25% collagenase at 37°C for 30 minutes. Cells were briefly stored at −80°C in 90% FBS and 10% DMSO. Cells were thawed, washed with PBS, and stained with TER-119 antibody. Dead cells and TER-119+ cells were excluded by sorting to enrich live non-erythroid cells. Single cell suspension at 300 cells/μL in PBS were subjected to Chromium 10x Genomics library construction and HiSeq2500 sequencing (The Genome Technology Access Center, Washington University in St. Louis).

ATAC-seq library generation, sequencing, and mapping

For ATAC-seq library generation, approximately 50,000 cKIT$^+$ cells were isolated from WT and *Baf155* CKO YS using FACS sorter as described above. ATAC-seq libraries were generated following the Omni-ATAC protocol (Corces et al., 2017) with the following modification: Cells were harvested by centrifuging at 500 g for 5 minutes at 4°C. Supernatant was carefully aspirated and cells were washed once with cold PBS. Cell pellets were lysed in 100 μl of ATAC-seq RSB (10 mM Tris pH 7.4, 10 mM NaCl, 3 mM MgCl$_2$) containing 0.1% NP40, 0.1% Tween-20, and 0.01% Digitonin by pipetting up and down and incubating on ice for 3 minutes. Next, 1 mL of ATAC-seq RSB containing 0.1% Tween-20 was added and mixed with the lysis reaction. Nuclei were pelleted by centrifuging at 800 g for 5 minutes at 4°C. Supernatant was carefully removed, and nuclear pellets were resuspended in 20 μl 2x TD buffer (20 mM Tris pH 7.6, 10 mM MgCl$_2$, 20% Dimethyl Formamide). Nuclei were counted using trypan blue. Approximately 50,000 nuclei were transferred to 25 μL of 2x TD buffer. 25 μl of transposition mix (2.5 μl transposase (100 nM final), 16.5 μl PBS, 0.5 μl 1% digitonin, 0.5 μl 10% Tween-20, and 5 μl H$_2$O) was then added to the nuclei. Transposition reactions were mixed and incubated at 37°C for 30 min gently tapping every 10 min to mix. Reactions were cleaned up with Zymo DNA Clean and Concentrator 5 columns. ATAC-seq library was prepared by amplifying the DNA for 9 cycles on a thermal cycler. The PCR reaction was purified with AMPure XP beads using double size selection following the manufacture's protocol, in which 27.5 μl beads (0.55x sample volume) and 50 μl beads (1.5x sample volume) were used based on 50 μl PCR reaction. ATAC-seq libraries were quantitated by Qubit assays. Paired-end ATAC-seq libraries were sequenced on an Illumina NextSeq 500 machine. The reads were de-multiplexed by using sample-specific index sequences. Nextera adaptor sequences were trimmed by using cutadapt (Martin, 2011) version 1.11. The trimmed reads were mapped to the mouse genome sequence by using bowtie2 (Langmead and Salzberg, 2012) version 2.3.4.1 with the following parameters: –local -k 4 -X 2000 –mm. Secondary alignment, multiply mapped reads, and PCR duplicated reads were removed from the total aligned reads.

QUANTIFICATION AND STATISTICAL ANALYSIS

scRNA-seq bioinformatics analyses

The sequenced reads were mapped to the GRCm38 assembly using Cell Range 2.0.1 (10x Genomics). Sample demultiplexing, barcode processing, and single-cell 3′ counting was performed using the Cell Ranger Single-Cell Software Suite (10x Genomics).

Cellranger count was used to align samples to the mm10 reference genome, quantify reads, and filter reads with a quality score below 30. The resultant files were input into Seurat for normalization across all samples and merging. The Seurat package in R was used for subsequent analysis (Butler et al., 2018). Cells with Mitochondrial content greater than 5 percent were removed for downstream analysis. Data were normalized using a scaling factor of 10,000, and nUMI was regressed with a negative binomial model. Principal component analysis was performed using the top 3000 most variable genes and t-SNE analysis was performed with the top 15 PCAs. Clustering was performed using the FindClusters function which works on K-nearest neighbor (KNN) graph model with the granularity ranging from 0.1-0.9 and selected 0.6 for the downstream clustering. For identifying the markers for each cluster, we performed differential expression of each cluster against all other clusters identifying negative and positive markers for that cluster

Identification of ATAC peaks
Filtered aligned ATAC-seq reads were used to map to the transposon insertion sites, and ATAC peaks were called from those insertion sites. First, ATAC-seq reads mapped to mitochondrial DNA were removed from the aligned reads. Both ends of the paired-end reads were then treated as two Tn5 insertion sites. Tn5 insertion sites were adjusted to reflect the actual binding center of transposons as follows. All reads mapped to the + strand were offset by +4 bp, and all reads mapped to the − strand were offset by −5 bp. The ATAC peaks were identified from these insertion sites by using the MACS2 (Zhang et al., 2008) version 2.1.1 callpeak function with the following parameters: -g mm --keep-dup all -B --SPMR --nomodel --extsize 73 --shift -37 -p 0.01 --call-summits. The ATAC-seq signals were visualized on the WashU Epigenome Browser (Zhou et al., 2011) as fold change over background using bedGraph tracks generated by using the MACS2 bdgcmp function with the following parameter: -m FE.

Identification and analyses of DARs
To identify DARs, DiffBind (Ross-Innes et al., 2012) version 2.6.6 was used on the union set of ATAC peaks with the following parameters: minOverlap = 1, fragmentSize = 1, summits = 0. DARs were defined as the ATAC peaks with fold change > 2 and P-value < 0.05. Unaffected accessible regions were defined as the ATAC peaks that are present both wild-type and *Baf155* CKO cells and that are also with fold change < 1.1 and P-value > 0.05 from DiffBind. Heatmaps of ATAC-seq signal levels of DARs along with their neighboring regions were plotted by using deepTools (Ramírez et al., 2016). Gene Ontology enrichment analysis on DARs and unaffected regions were performed using GREAT (McLean et al., 2010) version 4.0.4. Motif enrichment analysis on DARs was performed using HOMER (Heinz et al., 2010) version 4.8. HOMER scanned the sequences of DARs for known motifs, and calculated enrichment score P-values using a binomial test. The heatmap of the selected known motifs were plotted using fold enrichment against the background. HOMER also discovered *de novo* motifs with their best matches to a known motif in DARs.

Statistics
GraphPad Prism 8 software was used for performing statistical analysis and generating graphs/plots. Data are presented as mean with standard deviation for all the measurements. All experimental data were reliably reproduced in two or more individual biological replicates. Details of the statistical tests performed are given in the respective figure legends. p < 0.05 was considered statistically significant.

Supplemental Information

Requisite Chromatin Remodeling

for Myeloid and Erythroid Lineage Differentiation

from Erythromyeloid Progenitors

Jun Wu, Karen Krchma, Hyung Joo Lee, Sairam Prabhakar, Xiaoli Wang, Haiyong Zhao, Xiaoyun Xing, Rho H. Seong, Daved H. Fremont, Maxim N. Artyomov, Ting Wang, and Kyunghee Choi
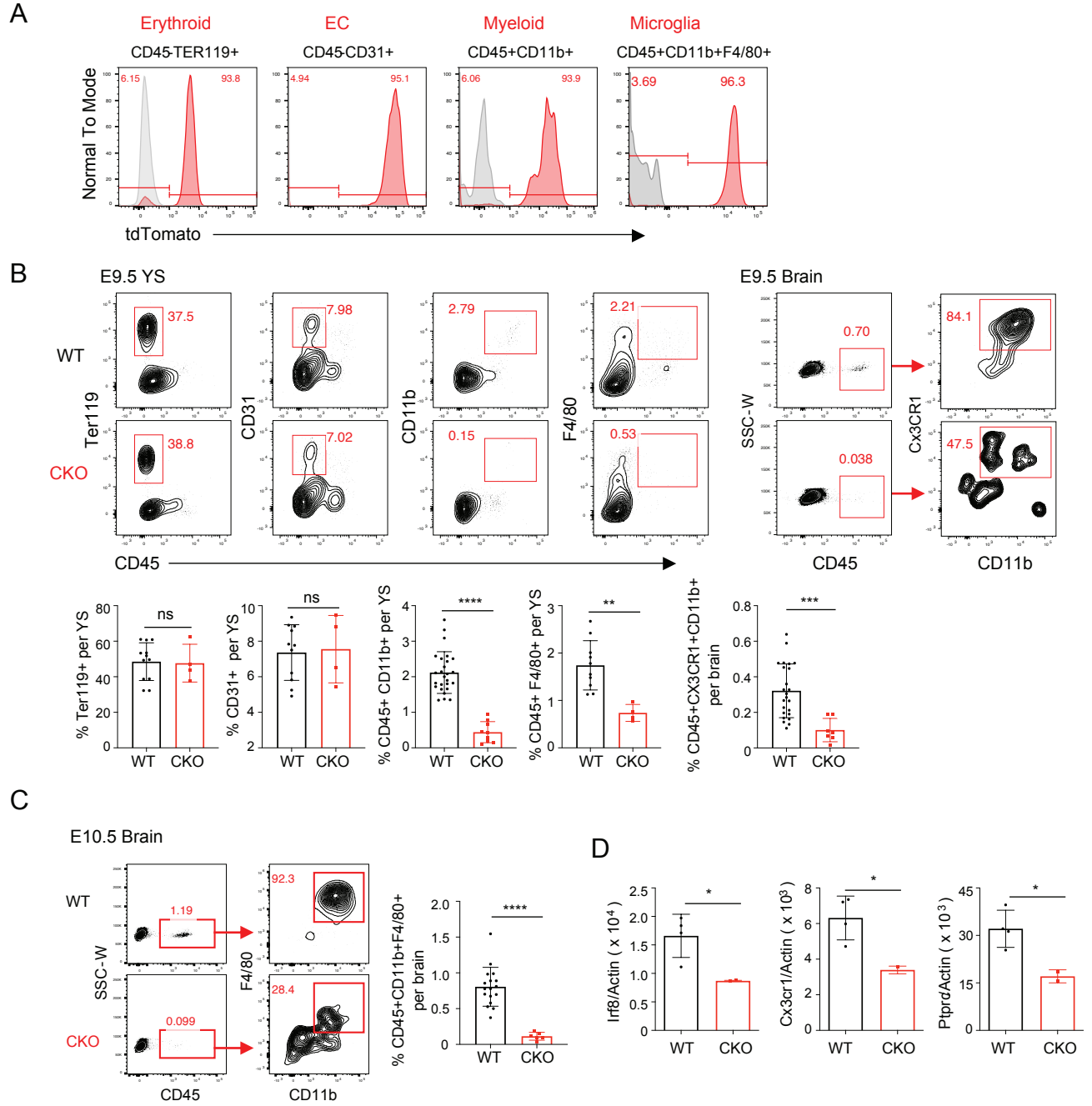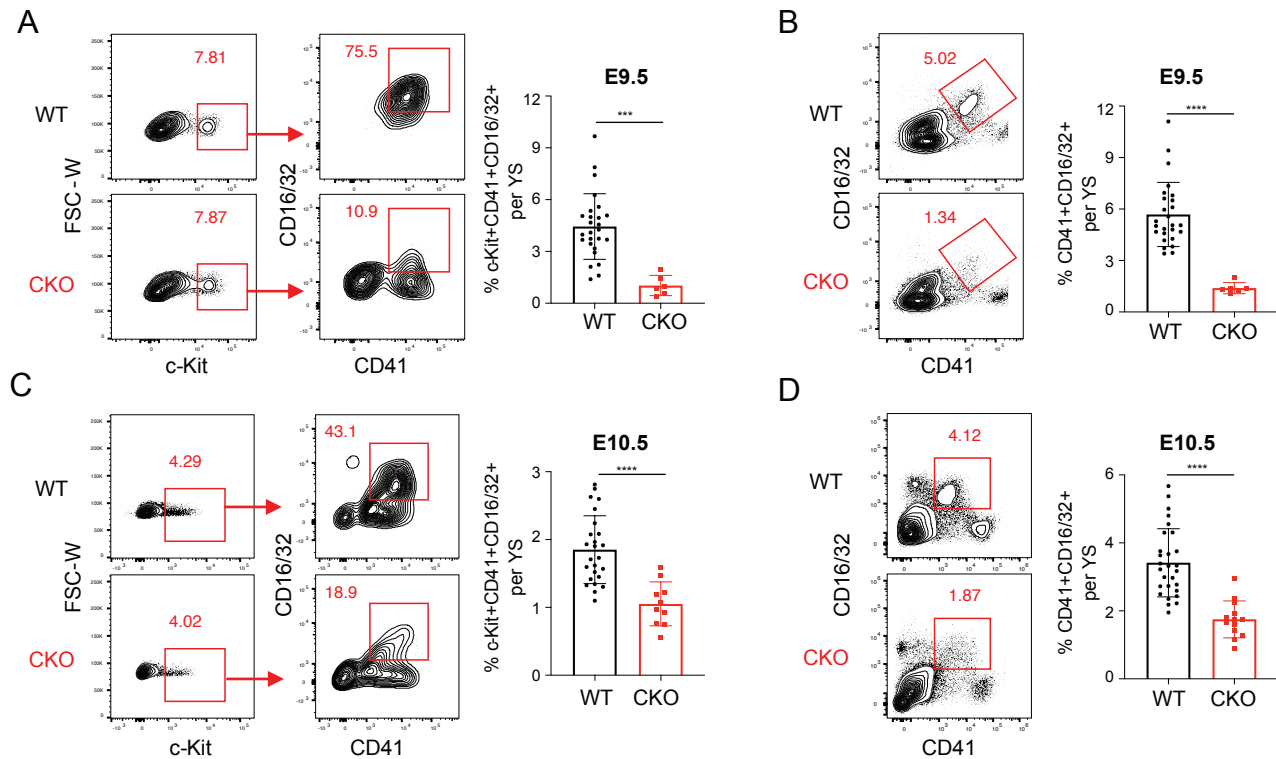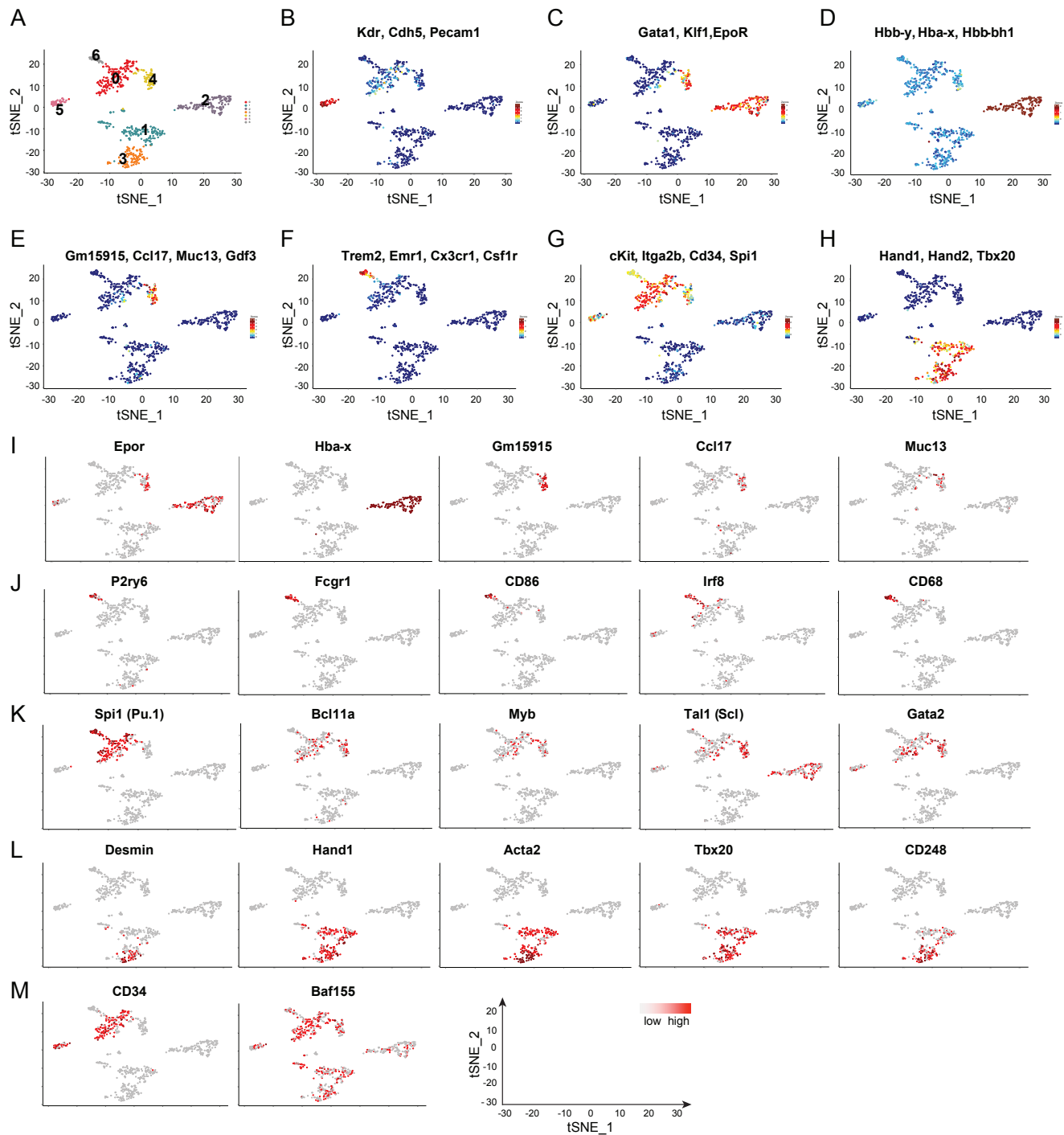
Figure S1

Figure S1 (Related to Figure 1). *Baf155* **CKO mice show defects in myeloid and definitive erythroid lineage development.**

(A) Flow cytometry analysis of erythroid cells (CD45$^-$TER119$^+$), endothelial cells (EC, CD45$^-$CD31$^+$), myeloid (CD45$^+$CD11b$^+$) and microglia (CD45$^+$CD11b$^+$F4/80$^+$) from E10.5 *Tie2*-Cre;Rosa26-floxed stop tdTomato YS and brain rudiment. **(B)** A representative flow cytometric analysis of E9.5 yolk sac (YS) primitive erythroid cells (CD45$^-$Ter119$^+$), endothelial cells (CD45$^-$CD31$^+$), myeloid cells (CD45$^+$CD11b$^+$), macrophages (CD45$^+$F4/80$^+$), and brain microglia (CD45$^+$CX3CR1$^+$ CD11b$^+$) in wild type (WT) and *Baf155* CKO mice is shown in the upper panel. The percentage of each population is shown in the bottom panel. At least 4 biological replicates in 2 independent experiments for either genotype were analyzed, each representing an individual YS. Data are presented as mean ± SD. Student's t-test. ns. not significant, **p<0.005. ***p<0.001. ****p<0.0001. **(C)** A representative flow cytometry analysis of microglia (CD45$^+$CX3CR1$^+$ CD11b$^+$) from E10.5 WT and *Baf155* CKO brain rudiments is shown in the left panel and percentage of microglia is shown on the right. At least 6 biological replicates for either genotype, with each replicate consisting of an individual embryo. Data are presented as mean ± SD. Student's t-test. *****p<0.0001.* **(D)** qRT-PCR analysis of indicated gene expression in E10.5 WT and *Baf155* CKO YS. Data from at least 2 biological replicates, with each replicate consisting of an individual YS. Data are presented as mean ± SD. Student's t-test. *p<0.05.*

Figure S2 (Related to Figure 2). *Baf155* **is required for myeloid and definitive erythroid lineage differentiation from EMPs.**

(A) An example of flow cytometry analysis of a Kit$^+$CD41$^+$CD16/32$^+$ population from E9.5 WT (top) and *Baf155* CKO (bottom) YS (left panel). Percentage of Kit$^+$CD41$^+$CD16/32$^+$ per YS is shown on the right. Data are presented as mean ± SD from 26 WT and 6 *Baf155* CKO biological replicates from 4 independent experiments. Student's t-test. ns. not significant, ***$p<0.001$. **(B)** An example of flow cytometry analysis of a CD41$^+$CD16/32$^+$ population from E9.5 WT and *Baf155* CKO YS (left). Percentage of CD41$^+$CD16/32$^+$ cells per YS is shown on the right. Data are presented as mean ± SD from 26 WT and 6 *Baf155* CKO biological replicates in 4 independent experiments. Student's t-test. ns. not significant, ****$p<0.0001$. **(C)** An example of flow cytometry analysis of a Kit$^+$CD41$^+$CD16/32$^+$ population from E10.5 WT and *Baf155* CKO YS (left). Percentage of Kit$^+$CD41$^+$CD16/32$^+$ cells per YS is shown on the right. Data are presented as mean ± SD from 26 WT and 10 *Baf155* CKO biological replicates in 4 independent experiments. Student's t-test. ns. not significant, ****$p<0.0001$. **(D)** An example of flow cytometry analysis of a CD41$^+$CD16/32$^+$ population from E10.5 WT and *Baf155* CKO (left) YS. Percentage of CD41$^+$CD16/32$^+$ cells per YS is shown on the right. Data are presented as mean ± SD from 28 WT and 13 *Baf155* CKO biological replicates in 7 independent experiments. Student's t-test. ns. not significant, ****$p<0.0001$.
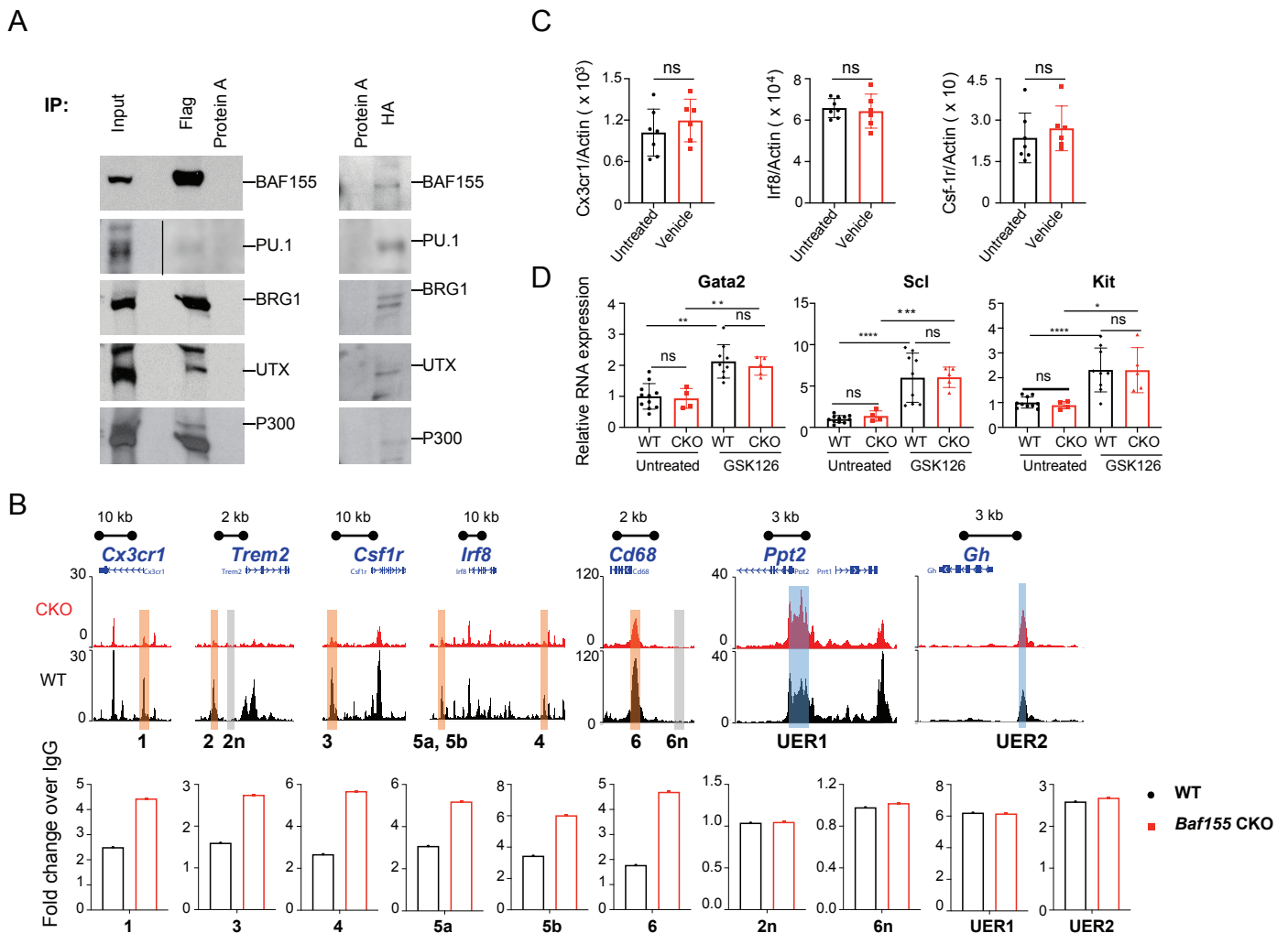
Figure S2

Figure S3 (Related to Figure 3). scRNA-seq of wild type yolk sac shows 7 independent cell populations.

(A) t-SNE projection of all cells, showing 7 different clusters. (B-H) Expression of the indicated marker genes for specific cell states/lineage fates in the t-SNE. B, endothelial cells; C, primitive and definitive erythroid cells; D, primitive erythroid cells; E, definitive erythroid cells; F, myeloid cells; G, EMPs; and H, pericytes and smooth muscle cells. (I) The expression of primitive and definitive erythroid cell markers in the t-SNE. (J) The expression of myeloid cell markers in the t-SNE. (K) The expression of EMP marker genes in the t-SNE. (L) The expression of pericytes and smooth muscle cell markers in the t-SNE. (M) CD34 and Baf155 expression in each cluster is shown.
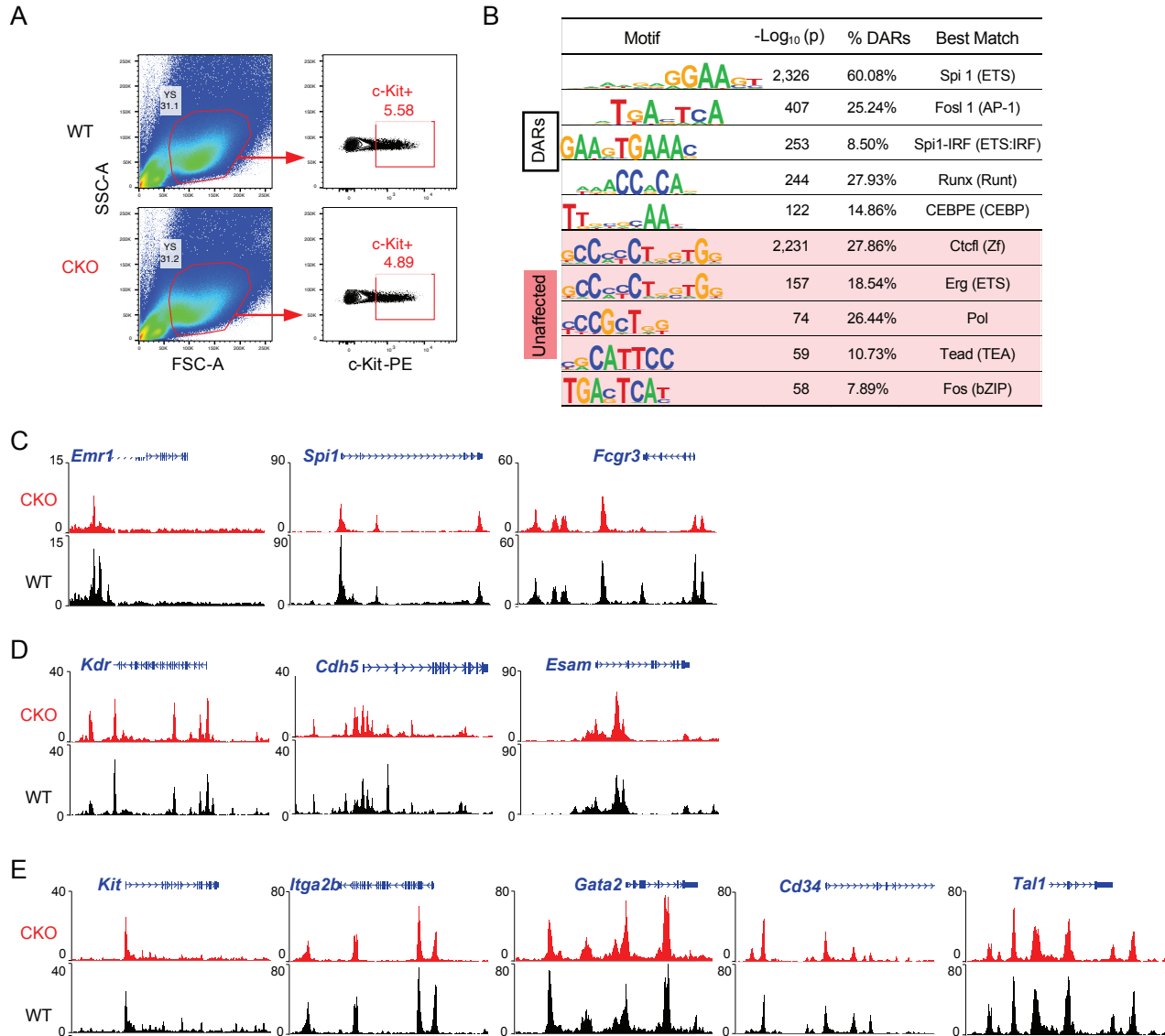
Figure S3

Figure S4 (Related to Figure 4). *Baf155* **CKO EMPs have reduced chromatin accessibility at the myeloid and EryD gene loci.**

(A) Gating strategy for isolating cKIT^{+} cells from WT (top) and *Baf155* CKO (bottom) YS. **(B)** Top 5 *de novo* transcription factor motifs enriched in the DARs with reduced signals in *Baf155* CKO EMPs (top) and in the unaffected regions (bottom). **(C)** Epigenome browser views of myeloid gene loci. **(D)** Epigenome browser views of EC gene loci. **(E)** Epigenome browser views of EMP gene loci.

Figure S5 (Related to Figure 5). BAF155 interacts with PU.1 and is recruited to its target genes.

(A) Nuclear extracts from MEF cells overexpressing Flag-*Baf155* and *Pu.1* or Flag-*Baf155* and HA-*Pu.1* were subjected to immunoprecipitation with anti-FLAG (left) or anti-HA affinity gel (right) and immunoblotted with BAF155, PU.1, BRG1, UTX and P300. Protein A agarose pull down serves as a negative control. **(B)** Epigenome browser views of selected myeloid and negative control genomic regions, and unaffected ETS regions between WT and *Baf155* CKO YS EMPs (top panel). ChIP-qPCR showing enrichment of H3K27me3 binding at selected myeloid gene loci (highlighted regions in top panel, 1-6), negative control gene loci (highlighted regions in top panel, 2n and 6n) and unaffected ETS regions (highlighted regions in top panel, UER1 and UER2) between E10.5 WT and *Baf155* CKO YS (bottom panel). qPCR primers and genomic locations are provided in Table S3. Sixty-three WT yolk sacs and 21 *Baf155* CKO yolk sacs were pooled together to perform ChIP. The average from three independent PCR data is shown. **(C)** qRT-PCR analysis of *Cx3cr1*, *Irf8* and *Csf-1r* gene expression from E9.5 wild type yolks sac with or without SBE- β-CD (GSK126 vehicle) treatment. Data from at least six biological replicates for each group. Data are presented as mean ± SD. Student's t-test. ns. not significant. **(D)** qRT-PCR analysis of *Gata2*, *Scl* and *Kit* gene expression from E9.5 WT and *Baf155* CKO YS with or without GSK126 treatment. Gene expression was normalized to untreated WT mean values. Data from at least 4 biological replicates for each genotype. Data are presented as mean ± SD. Student's t-test. ns. not significant, * *p<0.05*. ***p<0.01*. ****p<0.001*. *****p<0.0001*.

Figure S5

Table S1 (Related to Figure 1). Tie2-Cre:Baf155 CKO mice are embryonic lethal.

		# of Litters	Average Litter Size	# of pups	Expected # cKO	Tie2(+) Srg3 f/f	Tie2(-) Srg3 f/f	Tie2(+) Srg3 f/+	Tie2(-) Srg3 f/+
E9.5	Mating Scheme								
♂ Tie2(+) Srg3 f/+ x ♀ Srg3 f/f	Expected Desired Genotype (cKO) 25%	29	7.1	209	Expected 52.25	48	65	41	55
E10.5	Mating Scheme								
♂ Tie2(+) Srg3 f/+ x ♀ Srg3 f/f	Expected Desired Genotype (cKO) 25%	30	7.2	216	Expected 54	49	59	56	52
P21	Mating Scheme								
♂ Tie2(+) Srg3 f/+ x ♀ Srg3 f/f	Expected Desired Genotype (cKO) 25%	10	5.5	55	Expected 13.75	0	13	21	20